Mon. Not. R. astr. Soc. (1987) **225**, 903–937

The chromospheres and coronae of five G–K main-sequence stars

C. Jordan *Department of Theoretical Physics, University of Oxford, 1 Keble Road, Oxford OX1 3NP*

T. R. Ayres *Laboratory for Atmospheric & Space Physics, University of Colorado, Boulder, CO 80309, USA*

A. Brown and J. L. Linsky★ *Joint Institute for Laboratory Astrophysics, University of Colorado & National Bureau of Standards, Boulder, CO 80309-0440, USA*

T. Simon *Institute for Astronomy, University of Hawaii, 2680 Woodlawn Drive, Honolulu, HI 96822, USA*

Accepted 1986 November 12. Received 1986 November 10; in original form 1986 September 1

Summary. Five main-sequence stars, χ^1 Ori (G0V), α Cen A (G2V), ξ Boo A (G8V), α Cen B (K0V) and ε Eri (K2V) have been observed at low and high dispersion with the *International Ultraviolet Explorer* (*IUE*) satellite. The data obtained and X-ray observations reported in the literature are used here to make models of the structure of the atmospheres of these stars, from the high chromosphere to the corona. The electron pressures and coronal temperatures in these stars range from being similar to those in the quiet solar atmosphere (α Cen A) to the higher values found more typically in solar active regions (e.g. χ^1 Ori, ξ Boo A).

The models are used to examine the energy lost by radiation and transferred by thermal conduction, in order to establish the heating requirements. The results are similar to those found for the solar atmosphere. It seems unlikely that acoustic waves can provide sufficient flux above 2×10^4 K, but MHD modes cannot be excluded. Indeed, the observed emission measure distribution below 10^5 K can be matched in a model where Alfvén wave energy input, observed through non-thermal line broadening, is balanced by radiation losses. There are difficulties in disposing of energy conducted down from the corona – as in the Sun – difficulties which could in principle be resolved by restricting UV emission to supergranulation boundaries. There are not at present sufficient X-ray data to separate any time varying active region components from the 'average' corona.

★Staff Member, Quantum Physics Division, National Bureau of Standards.

Spherically symmetric coronae are adopted but modelling in terms of loops is also discussed and comparisons are made with other interpretations in the literature.

The coronal, transition region and chromospheric pressures are compared and show scaling relations which are compatible with previous flux correlations. A scaling between coronal pressure, temperature and gravity is found which agrees, on a relative scale, with the prediction of Hearn's minimum energy loss hypothesis. Comparisons are made with rotation flux correlations and in an exploratory manner these are related to the coronal magnetic field, pressure and temperature. A larger sample of stars and further observations are required to put these on a secure basis.

1 Introduction

Although many main-sequence stars are observable at low resolution using the *IUE* satellite, few are sufficiently bright to allow well-exposed spectra to be obtained at high resolution. Our programme of observations, aimed at understanding the energy balance in late-type main-sequence stars, has therefore concentrated on these objects, which tend to be unusually close or unusually active dwarfs.

The spectra obtained have been discussed in an earlier paper by Ayres *et al.* (1983, hereafter referred to as Paper I) and are reviewed briefly in Section 2. They include high-dispersion studies of χ^1 Orionis (G0V), ξ Boo A (G8V), and ε Eridani (K2V) all dwarfs with active chromospheres, and also the nearby binary system α Centauri A (G2V) and B (K0V), which is more similar to the Sun in activity. Here we use the data to make models of the structure of the chromospheres and coronae of the individual stars. The energy requirements of their atmospheres are examined and related to the presence of non-thermal motions deduced from the observed line profiles.

The methods for analysing the spectra of main-sequence stars are well established in the context of the solar atmosphere. The line fluxes are used to determine the emission-measure distribution. The electron density is found from density-sensitive line ratios (Section 4) and models of the structure are made assuming hydrostatic equilibrium (Section 5). In Section 3 the line fluxes and the models are then used to calculate the radiation losses and conductive flux and, since the main-sequence stars show no evidence for substantial mass loss, the energy input requirements are found (Section 6). Although it is necessary to adopt spherically symmetric uniform models as a first approximation, the effects of limiting the emission to restricted areas, analogous to solar active regions, are investigated. The line profiles are interpreted in terms of a non-thermal energy density to make comparisons between the energy required and that which could be carried in simple wave motions. The observed emission-measure distribution is compared with that predicted on the basis of an Alfvén wave flux, damped to match the observed non-thermal motions, and radiation losses.

In Section 7 comparisons are made between the observations and models for these stars and scaling laws which have been proposed to be more widely applicable. Some further correlations between pressure, coronal temperature and stellar rotation rates and mean magnetic fields are made in an exploratory manner.

Others have made models of the chromospheres of these stars or have modelled the X-ray emission in terms of closed magnetic loops. Comparisons are made with these results.

Although the emission-line fluxes are known to vary in some of the stars (e.g. χ^1 Ori), there are no systematic simultaneous studies of UV and X-ray fluxes available. The results of the present modelling are therefore assumed to refer to 'average' conditions. However, simultaneous studies of variability in different wavelength regions would enable constraints to be placed on the relative importance of the 'average' atmosphere and time varying active regions.

Table 1. Stellar parameters adopted.

Star	Spectral type	d^{a} (pc)	R_* ($R_\odot$)	g_* cm s^{-2}
χ^1 Ori	G0V	9.9	1.2	(2.2×10^4)
α Cen A	G2V	1.34	$1.1^{b,c}$	2.5×10^{4f}
ξ Boo A	G8V	6.9	0.98^{d}	2.5×10^4
α Cen B	K0V^{f}	1.34	$0.75^{b,c}$	4.5×10^{4f}
ε Eri	K2V	3.3	$0.82^{d,e}$	3.2×10^4

References
[a]Hoffleit (1964).
[b]Flannery & Ayres (1978) for mass.
[c]Kamper & Wesselink (1978) for mass.
[d]Ayres *et al.* (1983).
[e]Kelch (1978).
[f]Smith, Edvardsson & Frisk (1986).

The stellar parameters such as luminosities, magnitudes and rotational periods, have been discussed in Paper I. The distances, radii and gravities adopted are given in Table 1. For α Cen A and α Cen B we use determinations of gravity by Smith, Evardsson & Frisk (1986) and combine these with the earlier masses to revise the stellar radii. Demarque, Guenther & Van Altena (1986) and Guenther & Demarque (1986) have recently suggested values of M_* and R_* for α Cen A and ε Eri on the basis of observations of stellar oscillations and stellar structure models; their values agree with those listed in Table 1 to within 10 per cent.

2 Observations

The *IUE* observations of the five stars and in the subsequent data reduction have been discussed in Paper I which includes a catalogue of the image numbers and exposure times. The line fluxes and widths used in the analysis which follows are the same as in that paper unless otherwise stated. Some additional data are given in Tables 2 and 3.

Table 2. Surface fluxes and atomic parameters adopted and emission measures for χ^1 Ori.

Transition Ion	λ (Å)*	Flux erg cm^{-2} s^{-1}	Ω mult.	N_E/N_H	$\log T_m$ (K)	$\log \int_{\Delta R} N_e^2\,dh$ (cm^{-5})
Mg II	2800	3.9 (6)	17	5 (−5)	3.8	33.10
Si II	1817	1.2 (5)	15	4 (−5)	4.1	30.44
C II	1335	3.9 (4)	6.2	2.5 (−4)	4.2	29.40
Si III	1892	1.1 (4)	3.2	4 (−5)	4.7	27.95‡
Si IV	1400	5.7 (4)	16	4 (−5)	4.85	28.10
He II	1640	4.6 (4)	See text	0.065	4.95	29.26
C IV	1550	6.6 (4)	11	2.5 (−4)	5.0	27.45
N V	1240	<1.4 (4)†	7.2	8 (−5)	5.3	<27.55
C I	1657	5.5 (4)	See text		See text	
X-rays		8.8 (5)	See text		6.82	28.64

$^\star\lambda$ (multiplet) and total fluxes.
†From Simon, Herbig & Boesgaard (1985).
‡For $\log N_e = 11.50$.

Table 3. (a) Logarithmic scaling factors for $E_m(0.30)$, from those of χ^1 Ori.

Ion	ξ Boo A	ε Eri	α Cen A	α Cen B
Mg II	−0.10	−0.31	−0.75	−0.71
Si II	+0.03	−0.23	−0.82	−0.72
C II	+0.08	−0.18	−0.91	−0.77
Si III	−0.19	−0.29	−0.60	−0.70
Si IV	−0.25	−0.90	−1.36	−1.43
C IV	−0.11	−0.37	−1.09	−1.08
N V	−0.16	−0.53	>−1.17	>−1.27

(b) Scaling factors for surface fluxes; Δ log flux from those of χ^1 Ori.

Ion	ξ Boo A	ε Eri	α Cen A	α Cen B
He II	−0.09	−0.36	−2.20	−1.54
C I (1657 Å)*	[3.5 (4)] 0.0	−0.29	−0.55	−0.59
C I (1994 Å)*	[4.4 (3)] 0.0	−0.06	+0.08	−0.31
X-rays	+0.49	−0.26	−1.70	−1.03

*Based on given fluxes for ξ Boo A, since C I 1994 Å is not observed in χ^1 Ori.

X-ray fluxes are taken from the literature (see Paper I) but more recent results are included in Section 3(2) on X-ray emission measures.

The known properties of the stars from ground-based observations were discussed in Paper I and here we mention some more recent work. In particular, the activity of dwarf stars is almost certainly controlled by the properties of the magnetic field and attempts to measure photospheric fields have continued. The various types of measurements have been reviewed by Giampapa (1984) and Linsky (1985).

ξ Boo A has been more thoroughly studied than the other stars. Earlier work by Robinson, Worden & Harvey (1980) resulted in detections of fields of up to 2900 G covering ~40–45 per cent of the surface. Other reported detections include a mean field of ~1100 G over 67 per cent of the surface (Marcy 1984), and vector fields of ~25 G and 72 G (Borra, Edwards & Mayor 1984). However, non-detections are also reported (Marcy 1981; Gondoin, Giampapa & Bookbinder 1985). Whilst it is likely that ξ Boo A does have a variable magnetic flux, at present we have to model with uniform conditions, but simultaneous magnetic field and UV observations are planned.

Marcy (1984) also reports a mean field of ~1200 G over 67 per cent the surface on ε Eri, again with large variations in a few days (from ~620 G over ~88 per cent of the surface to ~2850 G over ~20 per cent of the surface). On the other hand, Saar, Linsky & Duncan (1986), using a new technique (*cf.* Saar, Linsky & Beckers 1986) that compensates for line blends and saturation, measure field strengths within the small range of 1700–2000 G and filling factors between 0.07 and 0.15. These results are based on 11 spectra of ε Eri obtained over 2 months.

Studies of rotational modulation of line fluxes, both in the optical (Ca II *H* and *K*) and UV, provide another way of estimating the relative contributions of activity. Of the stars treated here χ^1 Ori is the best observed to date (Boesgaard & Simon 1984). These authors found variations of up to a factor of 2.3 in C IV, but more typically these were ~±30 per cent, with evidence of variations in phase with rotation. Lines formed at lower temperatures do not show the phased variation and also vary by about ±30 per cent, but the Mg II flux shows no significant variation. Variations of about ±50 per cent will not substantially alter the interpetation in terms of an average atmosphere – one simply expects regions to be present with electron pressures or temperature gradients which differ by factors of $\sqrt{2}$ and 2, respectively, from the mean. Further rotational modulation studies would be of value and are planned for ξ Boo A.

3 Emission-measure distributions

3.1 EUV LINES

The methods of analysing the fluxes of effectively thin emission lines are now well established from early solar work, and have been described in the review by Jordan & Brown (1981).

The line flux is related to collision strength Ω, elemental abundance, N_E/N_H, and emission measure

$$\int_{\Delta R} N_e^2 \, dh,$$

by

$$F_{*12} = \frac{6.8\times10^{-22}}{\lambda} \frac{\Omega_{12}}{\omega_1} \frac{N_E}{N_H} \int_{\Delta R} N_e^2 g(T) \frac{N_1}{N_{\rm ion}} dh \quad \text{erg cm}^{-2}\,\text{s}^{-1}, \tag{1}$$

where λ is the wavelength in cm, ω_1 is the statistical weight of the lower level, $N_1/N_{\rm ion}$ is the fractional population of the lower level and $g(T)$ contains the main temperature-dependent terms in the line contribution function,

$$g(T) = \left(\frac{N_{\rm ion}}{N_E}\right) T_e^{-1/2} \exp\left(-\frac{W_{12}}{kT_e}\right) \tag{2}$$

where W_{12} is the line excitation energy and $N_{\rm ion}/N_E$ is the relative ion abundance. Although equations (1) and (2) are shown for a simple two-level atom, in practice full calculations of level populations are made. Below 2×10^4 K, $0.8\,N_e^2$ in equation (1) is replaced by $N_e N_H$.

Our calculations of level populations were brought up to date in application of the methods to T Tau (Brown, Ferraz & Jordan 1984) to β Dra (Brown *et al.* 1984) and α TrA (Hartmann *et al.* 1985). More recent work on Si II is discussed below. We adopt solar abundances except for elements heavier than He II in α Cen A and α Cen B for which we use values 1.58 times the solar values (Flannery & Ayres 1978; Smith *et al.* 1986).

Table 2 gives the lines used in the analysis, the temperature, T_m, at which the function $g(T)$ has its maximum value, the values of Ω and N_E/N_H adopted and the resulting emission measures at T_m for χ^1 Ori. In Fig. 1, we plot the *locus* of the emission measure $\int N_e N_H \, dh$ required if each line were *all* formed at a particular temperature. This has the advantage of giving an *upper limit* to the emission measure distribution, particularly at tempertures where there is a little overlap in the region of line formation and where the emission measure varies rapidly. However, we also show the emission measure

$$E_m(0.3) = \int_{\Delta R} N_e^2 \, dh, \tag{3}$$

where ΔR corresponds to a temperature range $\Delta \log T_e = 0.30$, which takes into account the fraction of the line flux formed over this temperature range.

The value of $\int_{\Delta R} N_e^2 \, dh$ for Si III lies below the corresponding locus of $\int N_e N_H \, dh$ because of the unusually broad contribution function of the line. We use the ion populations of Baliunas & Butler (1980), for the Si ions, calculated including charge exchange with hydrogen.

The only multiplet for which a new value of Ω is adopted since our previous calculations is

$3s^23p\,^2P$–$3s3p^2\,^2D$ in Si II with components at 1808, 1816 and 1817 Å. Level populations for Si II have recently been published by Dufton & Kingston (1985), in which a collision strength of $\Omega_{\rm total}\sim 15$ is used, a factor of 7 larger than the previous estimate provided by Tully (private communication). Such a large value of Ω accounts for the anomalous behaviour of the Si II lines in the density regime where excitation from the metastable quartet is unimportant. Excitations from the quartet level (Jordan 1969a), now become significant only at $N_e \geqslant 10^{11}\,{\rm cm}^{-3}$. The small

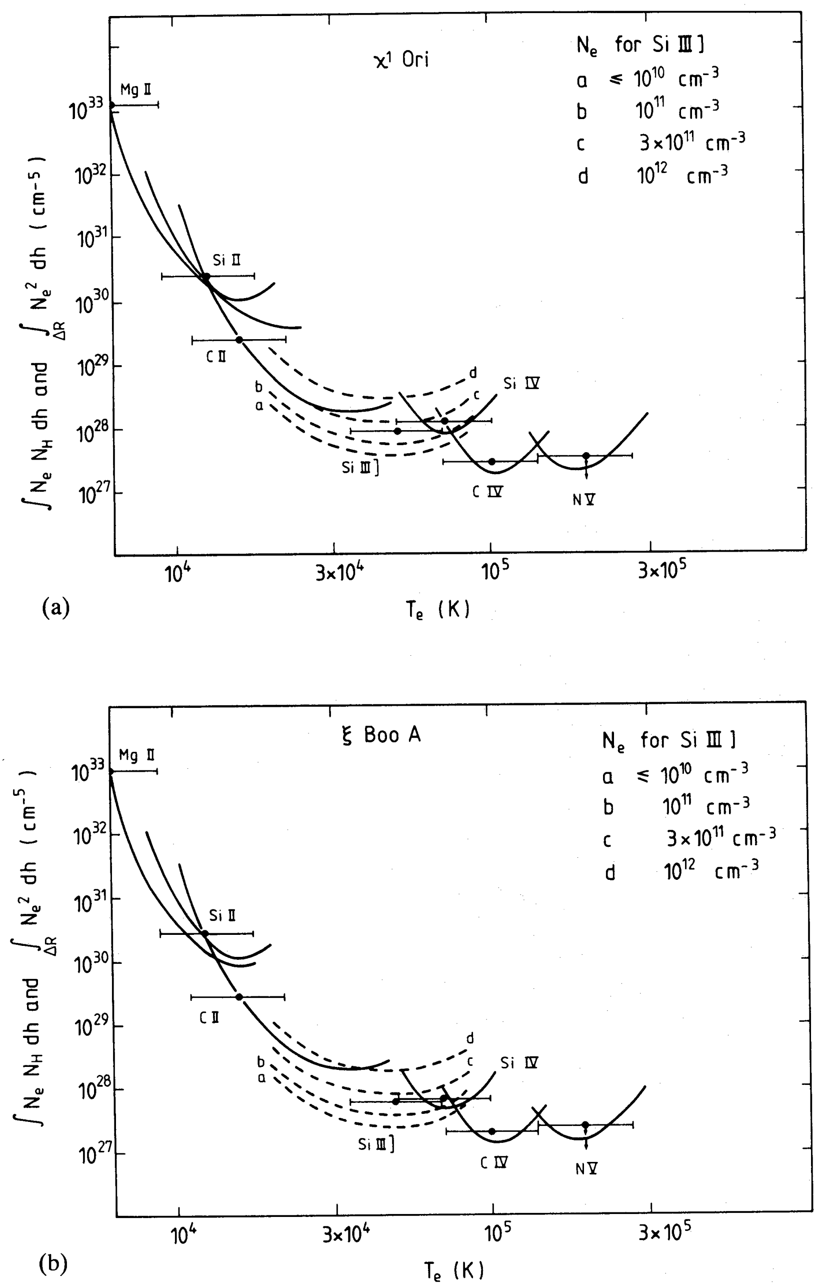

Figure 1. (a) Emission measure distribution for χ^1 Ori. The loci (full lines) of values of $\int N_e N_{\rm H}\,dh$ provide upper limits to the mean emission measure distribution. The values of $\int_{\Delta R} N_e^2\,dh$ are mean values required to give the observed line flux, centred on the temperature shown. The loci for Si III] (dashed lines) are shown for densities in the range of 10^{10}–$10^{12}\,{\rm cm}^{-3}$. (b) Emission measure distribution for ξ Boo A. Otherwise as for (a). (c) Emission measure distribution for ε Eri. Otherwise as for (a). (d) Emission measure distribution for α Cen A. Otherwise as for (a). (e) Emission measure distribution for α Cen B. Otherwise as for (a).

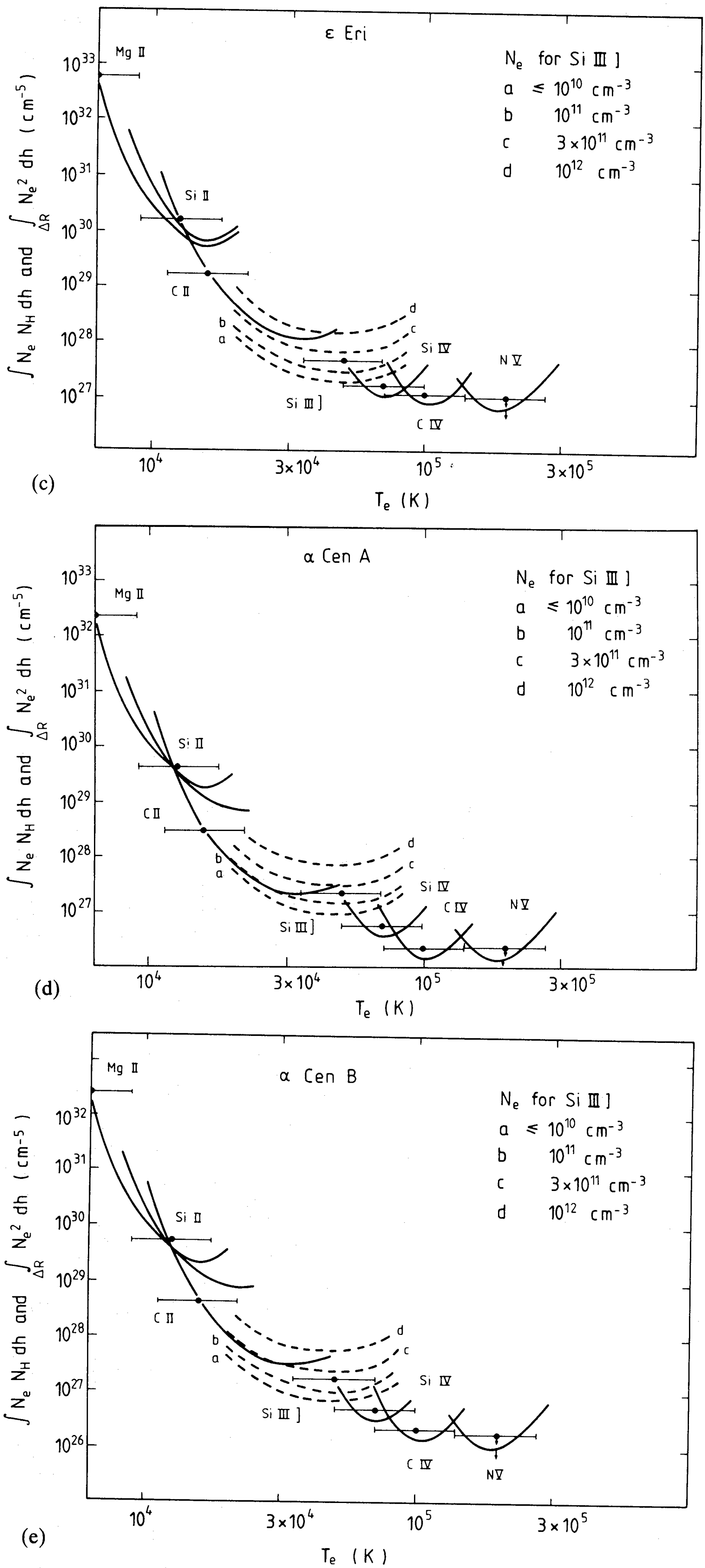

Figure 1–*continued*

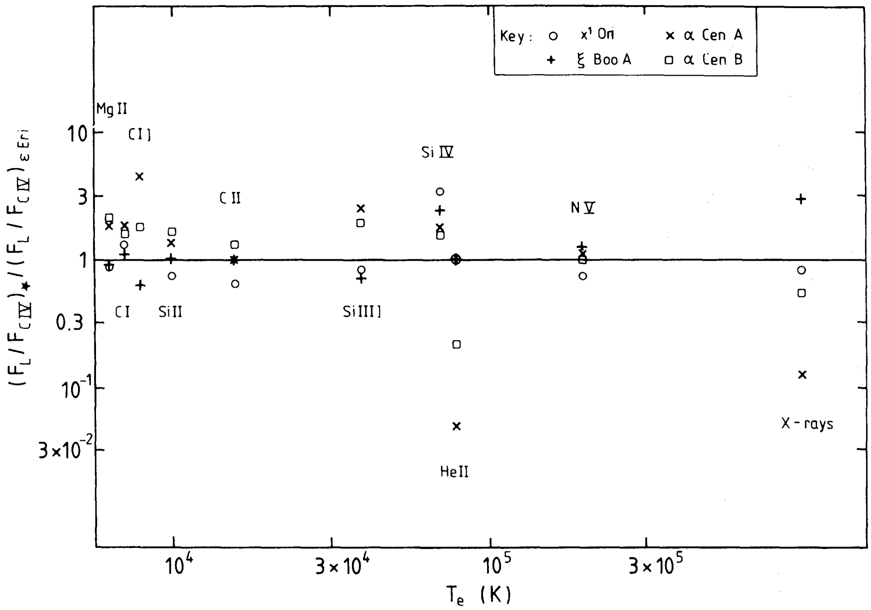

Figure 2. The ratio $(F_{\rm Line}/F_{\rm C\,IV})_*/(F_{\rm Line}/F_{\rm C\,IV})_{\varepsilon\,\rm Eri}$ as a function of temperature. The lines of C I and C I] are formed at $T_e \sim 6300$ K but are displaced in temperature for clarity. The temperatures for the X-ray emission are given in Table 5. Symbols are: ○, χ^1 Ori; +, ξ Boo A; □, α Cen A; ×, α Cen B.

A-value and large Ω for the ^2P–^2D transition will lead to significant collisional de-excitation of these lines at very high densities ($N_e \gtrsim 10^{12}$ cm^{-3}).

Fig. 1(a) shows the emission-measure distribution for χ^1 Ori, Fig. 1(b)–(e) those for the other stars. Because the distributions are very similar the differences between the five stars are brought out in Fig. 2 by plotting $[F(\text{Line})/F(\text{C IV})]^*/[F(\text{Line})//F(\text{C IV})]_{\varepsilon\,\rm Eri}$. Table 3 gives the factors by which $\Delta \log E_m$ may be scaled from the values for χ^1 Ori as listed in Table 2 and the relative fluxes for lines not used in determining E_m and also the relative X-ray fluxes. The measured X-ray surface fluxes, in contrast to the majority of the EUV resonance lines, differ by over an order of magnitude, but to interpret these fluxes the mean coronal temperature and *total* emission at all wavelengths must be considered.

For these stars the trend for $F(\text{C IV})/F(\text{Mg II})$ to increase with $F(\text{Mg II})^{1/2}$ (e.g. Ayres, Marstad & Linsky 1981) is roughly followed (see below). The lines for which the most obvious spread of ratios occurs are the C I] (1994 Å) and He II (1640 Å) transitions, and to a less significant degree the Si III] (1892 Å) transition. The C I] line is sensitive to the opacity in the resonance multiplet (1657 Å) and hence the ratio is related to $(N_e)^{-1}$, as is the ratio of Si III] to the resonance lines of other transition region ions. However, He II is sensitive to a combination of temperature gradient, opacity and soft X-ray ionizing flux and is proportional to some positive power of N_e. The flux ratio $F(\text{He II})/F(\text{C IV})$ does not take into account the higher metallicity in α Cen A and α Cen B and this contributes to the lower ratio for these stars in Fig. 2 (Flannery & Ayres 1978; Smith *et al.* 1986). These trends allow us to deduce that χ^1 Ori and ξ Boo A have the highest electron densities, whilst α Cen A and α Cen B have lower electron densities, irrespective of the *absolute* scale of the correlations.

Because Si III] 1892 Å is in the regime where its relative intensity to permitted lines is density sensitive, it is difficult to interpolate the emission measure accurately through the region around 3×10^4 K. The situation is complicated by the spread in the Si IV relative fluxes, as shown in Fig. 2. These fluxes are from high-resolution spectra and are not therefore contaminated by O IV blends. However, the ion balance of Si IV is sensitive to N_e through di-electronic recombination (see

Jordan 1969b) and Si IV is calculated to have an unusually low maximum ion abundance even at 'solar' densities (NSi IV/NSi $\sim 1/3$). It is possible that the ion abundance for Si IV should be larger – the maximum factor by which it could be raised is 3. We note also that there are no up-to-date calculations of the collision strength, Ω, for the Si IV resonance lines.

3.2 THE X-RAY EMISSION MEASURES AND MEAN CORONAL PARAMETERS

The X-ray fluxes and mean coronal temperatures have been taken from the following sources; for α Cen A and α Cen B we adopt the values given by Golub *et al.* (1982), who find a temperature of $2.1 \pm 0.4 \times 10^6$ K for the combined system, which is dominated by α Cen B. Models for α Cen A are made at two chosen temperatures, 2.1×10^6 K and 1.1×10^6 K. For ε Eri in Paper I we used a flux given by Johnson (1981). Both Giampapa *et al.* (1985) and Schrijver, Mewe & Walter (1984) have re-analysed data from the *Einstein Observatory*; their fluxes for ε Eri span the earlier value by $\sim \pm 15$ per cent. They find slightly different temperatures, Giampapa *et al.* give 3.4×10^6 K (no error bar quoted), Schrijver *et al.* find $2.3 \pm 0.2 \times 10^6$ K. Models are made for both temperatures. For ξ Boo A there are two values of the flux in the literature, originating from Walter (1981) and Walter *et al.* (1980). Pallavicini *et al.* (1981) suggest that the higher value (Walter 1981) is an overestimate and the value given by Walter *et al.* (1980) is adopted as in Paper I. The only temperature given in the literature is an 'estimate' of 10^7 K mentioned by Walter *et al.* (1980). For χ^1 Ori there are again two values of the flux in the literature, which differ by a factor of about 5. A flux of $\sim 4 \times 10^6$ erg cm^{-2} s^{-1} was adopted by Walter *et al.* (1980), Walter (1981) and Walter *et al.* (1984). However, both Schrijver *et al.* (1984), who also determine a temperature of $6.6 \pm 1.0 \times 10^6$ K and Simon, Herbig & Boesgaard (1985) find a flux of $\sim 8 \times 10^5$ erg cm^{-2} s^{-1}. The lower value is adopted since it is based on the final *Einstein* IPC calibration and emissivities consistent with those adopted below.

The coronal X-ray emission measure can be expressed in terms of the stellar surface flux, F_X, the radiative power loss, P_{rad}, (erg cm^3 s^{-1}) and the emission measure, E_{m}, through the relation

$$F_X = \frac{0.8}{2} E_{\mathrm{m}}(T_{\mathrm{c}}) P_{\mathrm{rad}}(T_{\mathrm{c}}) f(T_{\mathrm{c}}). \tag{4}$$

The factor of 1/2 allows for the flux emitted down from the corona to be consistent with the treatment of EUV lines. $P_{\mathrm{rad}}(T_{\mathrm{c}})$ is the power loss function and $f(T_{\mathrm{c}})$ is the fraction of the total power that is emitted in the *Einstein* IPC wavelength range 3–80 Å. After examining the calculations of $P_{\mathrm{rad}}(T_{\mathrm{c}})$ and $f(T_{\mathrm{c}})$ in the literature a combination of calculations by Kato (1976) and Raymond, Cox & Smith (1976) and by Summers & McWhirter (1979) is found to give a reasonably self-consistent treatment, i.e. the relation

$$P_{\mathrm{rad}}(T_{\mathrm{e}}) = 1.3 \times 10^{-19}\, T_{\mathrm{e}}^{-1/2}, \tag{5}$$

is adopted between 2×10^5 and 10^7 K and the values of $f(T_{\mathrm{c}})\, T_{\mathrm{c}}$ as given in Table 4. In view of recent work by Schrijver *et al.* (1984) who adopt

$$F_X = 1.7 \times 10^{-23} E_{\mathrm{m}}(T_{\mathrm{c}}), \qquad \text{for } T_{\mathrm{c}} \sim 2 \times 10^6\ \mathrm{K} \tag{6}$$

and

$$F_X = 1.2 \times 10^{-23} E_{\mathrm{m}}(T_{\mathrm{c}}), \qquad \text{for } T_{\mathrm{c}} \sim 2 \times 10^7\ \mathrm{K} \tag{7}$$

based on emissivity calculations by Mewe & Gronenschild (1981), comparisons have been made between their results and our own for χ^1 Ori, ε Eri, α Cen A and α Cen B. For the two sets of

Table 4. Adopted values of $f(T_c)\,T_c$.

$\log T_e$ (K)	$\log f(T_c)\,T_c$ (K)
6.0	5.3
6.2	5.8
6.3	6.0
6.5	6.4
6.8	6.8
7.0	7.0

calculations to be consistent taking into account a factor of 0.8/2 difference in the definition of F_X and E_m one expects

$$f(T_c)\,T_c = 3.3\times10^{-4}\,T_c^{3/2} \qquad (T_c \sim 2\times10^6\,\mathrm{K}) \tag{8}$$

and

$$f(T_c)\,T_c = 2.3\times10^{-4}\,T_c^{3/2} \qquad (T_c \sim 2\times10^7\,\mathrm{K}). \tag{9}$$

Between 1.3 and 20×10^6 K our calculations agree to within 20 per cent, only below 10^6 K do larger differences appear. Of the stars discussed here only α Cen A is likely to have such a low average coronal temperature. We note in passing that the labels for α Cen A and α Cen B are interchanged in fig. 3(a) of Schrijver *et al.* (1984).

The value of $E_m(T_c)$ for χ^1 Ori found from equation (4) is given in Table 2. Scaling factors for the other stars are given in Table 3. The available mean coronal temperature estimates are given in Table 5.

The mean coronal emission measure can be used to find the average density and pressure, assuming that the emission is formed in a spherically symmetric corona close to the stellar surface, as is a good approximation for the average quiet solar corona. [Solar active regions only cause shorter term variability at temperatures *higher* than the average coronal temperature of $\sim1.5\times10^6$ K. This was shown from early whole Sun soft X-ray spectra (e.g. Neupert 1965).]

We write

$$E_m(T_c) = \int_{\Delta R} N_e^2\,dh = \bar{N}_c^2\,\Delta H, \tag{10}$$

where $\Delta H = 7\times10^7\,T_c g_*^{-1}$ is the isothermal scale height for the density squared and $\bar{N}_c^2$ is the mean square coronal density. The resulting values of $(N_c^2)^{1/2}$ and $P_c/k = (N_c^2)^{1/2}\,T_c$ are given in Table 5 at the best estimates for T_c. From equations (4), (5), (8) and (9) it can be seen that for a given measured F_X, $(\bar{N}_c^2)^{1/2}$ is approximately $\propto T_c^{-1/2}$ and P_c is approximately $\propto T_c^{1/2}$. Thus an

Table 5. Mean coronal electron densities and pressures.

Star	T_c (10^6 K)	$(\bar{N}_c^2)^{1/2}$ (cm^{-3})	P_c/k (cm^{-3} K)
χ^1 Ori	6.6	1.4 (9)	9.5 (15)
ξ Boo A	10	2.4 (9)	2.4 (16)
ε Eri	2.3 (a)	2.2 (9)	5.0 (15)
	3.4 (b)	1.6 (9)	5.6 (15)
α Cen A	1.1 (a)	5.7 (8)	6.3 (14)
	<2.1 (b)	>3.1 (8)	~6.6 (14)
α Cen B	2.1	9.0 (8)	1.9 (15)

uncertainty of $\pm\sqrt{2}$ in T_c leads to only about ± 20 per cent uncertainties in N_c and P_c. If, however, the observed emission originated in a more restricted volume, all the values of N_c and P_c/k in Table 5 would be lower limits.

4 Lines offering density diagnostics

Before proceeding with modelling based on coronal pressures the density and pressure estimates which can be made from UV line fluxes are discussed.

4.1 THE INTERSYSTEM LINES OF C III (1909 Å) AND Si III (1892 Å)

Both the low- and high-resolution spectra show that the intersystem line of C III at 1909 Å is very weak compared to the Si III intersystem line at 1892 Å. A ratio of FC III]/FSi III]$\lesssim 0.2$, which is a generous upper limit for ξ Boo A, χ^1 Ori and ε Eri, implies $N_e > 2.5\times10^{10}\,\mathrm{cm^{-3}}$ at $T_e \sim 5.5\times10^4$ K, i.e. $P_e/k > 1.4\times10^{15}\,\mathrm{cm^{-3}\,K}$. This lower limit is consistent with the X-ray lower limits but is not otherwise very useful. For α Cen B, Ayres *et al.* (1982) give a ratio of 0.15 ± 0.04, but note that the C III] flux is uncertain. This value gives $N_e = 4\times10^{10} \pm 2\times10^{10}\,\mathrm{cm^{-3}}$, or $P_e/k = 2.2\pm1.1\times10^{15}\,\mathrm{cm^{-3}\,K}$. It will be seen below that this value is compatible with the X-ray lower limit. In α Cen A the flux ratio appears to be larger and the best estimate is 0.5 ± 50 per cent. The resulting density and pressures are $N_e = 10^{10}\,\mathrm{cm^{-3}}$ (± 50 per cent) and $P_e/k = 5.5\times10^{14}\,\mathrm{cm^{-3}\,K}$ (in range 2.2×10^{14} to $1.1\times10^{15}\,\mathrm{cm^{-3}\,K}$), again compatible with the X-ray values. The source of uncertainty in α Cen A is some saturation of the Si III] line and the high level of the underlying continuum.

If the pressure regimes given by the X-ray fluxes are correct then at $T_e \sim 5\times10^4$ K the Si III] line emissivity should be in its low-density limit in α Cen A, but be sensitive to N_e in χ^1 Ori and ξ Boo A. The absolute flux in Si III] can be used to find the emission measure as a function of N_e, using the calculations by Dufton *et al.* (1983). From Fig. 1(a), it can be seen that with $N_e \lesssim 10^{10}\,\mathrm{cm^{-3}}$ the Si III] point would lie below the mean curve (taking the Si IV value into account), whereas a value of $N_e \sim 10^{12}\,\mathrm{cm^{-3}}$ will not fit the C II constraint. Matching the Si III] locus on to the C II locus suggests $N_e \sim 3\times10^{11}\,\mathrm{cm^{-3}}$ ($P_e/k \sim 1.5\times10^{16}\,\mathrm{cm^{-3}\,K}$, consistent with the X-ray value.) From Fig. 2 (or the numbers in Table 3) it can be seen that $N_e \sim 10^{12}\,\mathrm{cm^{-3}}$ would be required in ξ Boo A and $N_e \sim 10^{11}\,\mathrm{cm^{-3}}$ in ε Eri, but that because of the lower Si IV and C IV points, lower densities, $<10^{11}\,\mathrm{cm^{-3}}$, would give the best fit to the mean distributions for α Cen A and α Cen B. The ranges of acceptable densities from Si III] are summarized in Table 6.

4.2 THE C I INTERSYSTEM LINES

The intersystem line of C I $2p^2\,{}^1D_2$–$2p3s\,{}^3P_1^0$ (mult. UV 32) at 1993.62 Å is observed in all the stars except χ^1 Ori. This line is pumped by photons trapped in the optically thick multiplet

Table 6. Range of P_e ($\mathrm{cm^{-3}\,K}$) from Si III] flux and local emission measure.

Star	P_e/k ($\mathrm{cm^{-3}\,K}$)
χ^1 Ori	5 (15) to 2.5 (16)
ξ Boo A	1.5 (16) to 5 (16)
ε Eri	5 (15) to 1.5 (16)
α Cen A	≲5 (14) to 5 (15)
α Cen B	5 (14) to 5 (15)

(UV 2), $2p^{2}\,^3P$–$2p3s\,^3P^0$, for which a flux is also available. The ratio of the lines at 1993.62 and 1657.38, 1658.12 and 1656.93 Å (transitions from $3s\,^3P_1^0$) can be used to measure the opacity in the $2p^2\,^3P$–$2p3s\,^3P$ transition (Jordan 1967), and hence an approximate value of the mass column density $\int N_{\mathrm{H}}\,dh$ through and above the region where C I is formed can be found, as outlined below.

Since the lines decay from a common upper level, the ratio and their fluxes can be written as

$$F(1994)/F(1657)=1657\,b_1q_1/1994\,b_2q_2 \tag{11}$$

where b_1 is the branching ratio for the transition probability and q is the probability per emission of a photon escaping from the atmosphere. q can be expressed as (see Jordan 1967 for details)

$$q=1-\mathrm{erf}\,(\ln\tau_0)^{1/2} \tag{12}$$

where τ_0 is the opacity to the centre of the emitting region such that

$$\tau_0=6\times10^{-15}\lambda\,(\text{Å})\,f_{12}M^{1/2}\,\frac{N_{(\mathrm{E})}}{N_{(\mathrm{H})}}\int_{ho}^{\infty}\frac{N_1}{N_{(\mathrm{ion})}}\,\frac{N_{\mathrm{H}}}{T_{\mathrm{i}}^{1/2}}\,dh. \tag{13}$$

We adopt $N(\mathrm{E})/N(\mathrm{H})=2.5\times10^{-4}$, (or 3.9×10^{-4} for α Cen A and α Cen B) $N_1/N_{(\mathrm{Ion})}=1/3$, $T_{\mathrm{i}}=8000$ K, and assume NC I/NC II$=1.0$. M is the atomic weight. Nussbaumer & Storey (1984) have recently recalculated the oscillator strengths for C I. Their value for the 1657 multiplet is 40 per cent larger than that of Tatum (1968), used by Jordan (1967), but their value for the intersystem line at 1994 Å is identical with that of Tatum.

The values of $\int N_{\mathrm{H}}\,dh$ derived are given in Table 7. The largest uncertainty comes from the assumption that $N_{\mathrm{C\,I}}/N_{\mathrm{C\,II}}=1.0$ where the resonance lines are formed and since smaller values could result if carbon were more ionized the values given are lower limits.

The emission measure cannot be easily determined from the C I absolute flux owing to the

Table 7. (a) Estimates of $\int_{h0}^{\infty} N_{\mathrm{H}}\,dh$, N_{e} and N_{H} from C I ratios and Mg II fluxes.

Star	$\int_{h0}^{\infty} N_{\mathrm{H}}\,dh^{\star}$ (cm^{-2})	$\int_{\Delta R} N_{\mathrm{e}}N_{\mathrm{H}}\,dh$ (cm^{-5})	$\bar{N}_{\mathrm{e}}$ (cm^{-3})	N_{H} (at 6500 K) (cm^{-3})	$\sqrt{P_{\mathrm{e}}P_{\mathrm{H}}}/k$ (cm^{-3} K)
χ^1 Ori	–	1.0 (33)	–	–	4.0 (16)
ξ Boo A	2.8 (20)	8.1 (32)	2.9 (12)	1.3 (13)	3.8 (16)
ε Eri	4.6 (20)	5.0 (32)	1.1 (12)	2.5 (13)	3.3 (16)
α Cen A	6.3 (20)	1.8 (32)	2.8 (11)	2.8 (13)	1.7 (16)
α Cen B	3.2 (20)	1.9 (32)	6.1 (11)	2.5 (13)	2.4 (16)

(b) Values of N_{e}, N_{H} and $\sqrt{P_{\mathrm{e}}P_{\mathrm{H}}}$ at 6500 K from calculated models.

Star	N_{e} (cm^{-3})	N_{H} (cm^{-3})	$\sqrt{P_{\mathrm{e}}P_{\mathrm{H}}}/k$ (cm^{-3} K)
χ^1 Ori	9.3 (11)	1.9 (13)	2.6 (16)
ξ Boo A	2.2 (12)	6.4 (12)	2.4 (16)
ε Eri	6.4 (11) (b)	1.8 (13)	2.2 (16)
α Cen A	2.1 (11) (a)	1.5 (13)	1.1 (16)
α Cen B	3.4 (11)	1.9 (13)	1.6 (16)

*No particular value is assigned to h_0.
†From Mg II fluxes.

complexity of excitation and formation of the line over an undetermined temperature range and a value is derived by assuming that Mg II is formed predominantly around 6500 K. There is some basis for this from the models of ε Eri (Simon, Kelch & Linsky 1980) and solar models (VAL III, Vernazza, Avrett & Loeser 1981). The emission measure $\int_{\Delta R} N_e N_H \, dh$ is then divided by $\int N_H \, dh$ to give N_e. Although N_H varies rapidly with temperature, the models of α Eri and the Sun show that to within a factor of about 2, N_e varies slowly around 6500 K. Although one cannot expect the absolute values of N_e to be more accurate than about a factor of 3, it is found that the *relative* values of N_e (and P_e) follow the same order as do the coronal pressures, increasing from α Cen A to ξ Boo A.

To find a mean N_H a further assumption is required which is that Δh corresponds to the isothermal scale height at 6500 K. This is very crude since N_H varies rapidly with T_e. The values of N_H and $(P_e P_H)^{1/2}$ derived are given in Table 7 but should be regarded only as order of magnitude estimates.

Equation (13) can be used with the mass column densities to show that the opacity in the Mg II line in α Cen A is predicted to be a factor of 2 higher than in α Cen B. This is consistent with the high-resolution profiles of the Mg II lines observed by Ayres & Linsky (1980). Although the fluxes are very similar, the profiles in α Cen are distinctly self-reversed, whereas this is barely the case for α Cen B. Since $\tau \propto \int N_H \, dh$ and the flux $F \propto \int N_e N_H \, dh$ the essentially identical fluxes but higher opacity in α Cen A show that N_e is lower in α Cen A than α Cen B.

5 Models of the atmospheres

5.1 FROM EMISSION-MEASURE MODELLING

The method of using the emission-measure distribution, combined with hydrostatic equilibrium to determine the structure of stellar transition regions and coronae has been set out by Jordan & Brown (1981) and applied to several stars. Briefly, above $T_e \sim 2 \times 10^4$ K the emission measure is re-written to give the local temperature gradient

$$\frac{dT_e}{dh} = \frac{\bar{P}_e^2}{\sqrt{2}\, E_m(0.3)\, T_e} \tag{14}$$

(where P_e is in units of cm^{-3} K).

In these high-gravity stars the pressure scale heights are sufficiently small compared with the stellar radii to justify plane-parallel models.

Hydrostatic equilibrium gives

$$\frac{dP_e}{dh} = -7.1 \times 10^{-9} P_e g_* T_e^{-1}. \tag{15}$$

Equations (14) and (15) combine to give

$$P_e^2 = P_{\mathrm{Top}}^2 + 2.0 \times 10^{-8} g_* \int_{T_e}^{T_{\mathrm{Top}}} E_m(0.3)\, dT_e \tag{16}$$

where the subscript Top refers to the top of the atmosphere, where $T_{\mathrm{Top}} = \sqrt{2}\, T_c$, P_e and T_e are then determined as a function of height above a chosen reference level, provide a boundary condition on P_e is known.

The mean emission measure for χ^1 Ori is given in Table 8. Below 10^5 K this is based on the UV

Table 8. Mean emission measures and model for χ^1 Ori.

$\log T_e$	$\log E_m$ (0.30)	P_e/k (10^{16} cm^{-3} K)	$\log T_e$	$\log E_m$ (0.30)	P_e/k (10^{16} cm^{-3} K)
3.8	33.1	2.6*	5.1†	27.1	1.1
3.9	31.5	1.1*	5.2	26.8	1.1
4.0	30.7	0.97*	5.3†	26.4	1.1
4.1	30.2	0.96*			
4.2	29.4	0.95*	6.8	28.6	0.95
4.3	28.7	0.95*			
4.4	28.3	1.1			
4.5	28.1	1.1			
4.6	28.0	1.1			
4.7	27.9	1.1			
4.8	27.8	1.1			
4.9	27.7	1.1			
5.0	27.5	1.1			

*$(P_e P_H)^{1/2}/k$ below 2×10^4 K.
†Between $\log T_e=5.3$ and 6.8 we adopted $E_m/(T_e)=E_m(T_c)(T_e/T_c)^{3/2}$.
Between $\log T_e=5.0$ and 5.3 a linear interpolation is made.
T_e (K) and $E_m(0.3)$ (cm^{-5}) throughout.

line fluxes, and the mean curve reproduces all the line fluxes to within ±20 per cent apart from Si IV. Above 2×10^5 K we assume

$$E_m(T_e)=E_m(T_c)(T_e/T_c)^{3/2}$$

based on the behaviour of the solar emission measure (e.g. Jordan 1976, 1980). Between 10^5 and 2×10^5 K a linear interpolation is made. The starting pressure for equation (16) is taken as the 'coronal' value given in Table 5. The resulting pressures are given in Table 8; the model has essentially constant pressure down to $\sim10^4$ K.

The parameters which summarize the models for the other stars are given in Table 9. Equations (14), (15) and the $\Delta \log E_m$ factors in Table 3 can be used to determine the other models. Some general conclusions can be drawn from Table 9. For all the stars the pressure drops little above

Table 9. Parameters describing models.

Star	$\log T_c$ (K)	P_e/k* (10^{16} cm^{-3} K) at $\log T_e$ 3.8	5.3	at $\log T_c$	a† (cm^{-5} K$^{-3/2}$)
χ^1 Ori	6.82	2.6	1.1	0.95	2.5 (18)
ξ Boo A	7.00	3.2	2.7	2.4	5.2 (18)
ε Eri	6.36 (a)	2.2	0.56	0.50	7.0 (18)
	6.53 (b)		0.62	0.56	3.2 (18)
α Cen A	6.05 (a)	1.1	6.9 (−2)	6.3 (−2)	8.5 (17)
	6.32 (b)		7.3 (−2)	6.6 (−2)	1.9 (17)
α Cen B	6.32	1.6	0.21	0.19	8.8 (17)

*$(P_e P_H)^{1/2}$ at 6500 K.
†$a=E_m(T_e)/T_e^{3/2}$, $T_e>2\times10^5$ K.

$T_0=2\times10^5$ K and P_0 is $\sim1.1\,P_c$. This result follows from the use of a power law fit to $E_m(0.3)$ between T_0 and T_c and depends on the definition of $T_{Top}=\sqrt{2}\,T_c$, where T_c is the maximum observed temperature, and $P_{Top}\rightarrow0$ at T_{Top}. The factor of $\sqrt{2}$ is chosen since typically coronal lines are formed over a factor of 2 in temperature about their optimum temperature of formation. Then

$$\frac{P_0^2}{P_c^2}\rightarrow1+\frac{\sqrt{2}}{(b+1)}\times\left(\frac{1}{\sqrt{2}}\right)^{b+1}. \tag{17}$$

This pressure ratio changes slowly with $b\,(0\leqslant b\leqslant3)$. Between 10^5 and 10^4 K the pressure gradually rises as the second term in equation (16) becomes more important, but as can be seen from Fig. 1 the main increase in E_m occurs below 10^4 K. Then the second term in equation (16) dominates so that the base 'pressure' depends almost entirely on the Mg II flux.

Below $T_e\sim2\times10^4$ K the approximation $N_H=0.8\,N_e$ adopted in equation (1) becomes invalid. It is then more convenient to write

$$E'_m(0.3)=\int_{\Delta R}N_eN_H\,dh$$

and to work in terms of

$$\overline{\frac{dT_e}{dh}}=\frac{P_eP_H}{\sqrt{2}\,T_e}\,\frac{1}{E'_m(0.30)}. \tag{18}$$

Writing the equation of hydrostatic equilibrium in terms of $P_{total}=P_T$ where

$$P_T=P_e+P_H=P_e\left(1+\frac{P_H}{P_e}\right)=P_e(1+x)$$

leads to a revised second term in equation (16) such that

$$\Delta(P_T^2)=3.3\times10^{-8}\mu g_*\int_{T_1}^{T_2}E'_m(0.3)\left(\frac{1+x}{x}\right)^2dT_e \tag{19}$$

where μ is the mean molecular weight.

The individual values of N_e, N_H and N_T cannot be found without further assumptions. Based on the VAL III models for the solar atmosphere (Vernazza *et al.* 1981), we assume that $N_H=0.8\,N_e$ at $T_e>2\times10^4$ K, $N_H=N_e$ at 2×10^4 K, $N_e=0.75\,N_H$ at 10^4 K, $N_e=0.50\,N_H$ at 8000 K and $N_e=$const below 8000 K. The resulting values of N_e, N_H and $\sqrt{P_eP_H}$ are given in Table 7(b), where they can be compared with the numbers that were derived from the C I and Mg II line fluxes. The values of $\sqrt{P_eP_H}$ are in reasonable agreement because both values are dominated by the Mg II flux. For this reason too only one model is given for ε Eri and α Cen A. However, there is no *a priori* reason why the values of N_e and N_H should agree since those in Table 7(a) are based on the C I and Mg II fluxes, whilst those in Table 7(b) depend on X-ray and UV fluxes and the ratios of N_H/N_e adopted above. The agreement of the values to within a factor of 2 is therefore encouraging.

We stress that the emission measure between $\sim$6500 and 2.0×10^4 K is not very well determined and that, as discussed in Section 3.1 the loci plotted in Fig. 1 give only upper limits to E_m. The mean emission measure does reproduce the flux in the Si II and C II lines but a very rapid decrease in E_m above 6300 K rising again to match that shown around 1–2×10^4 K cannot be excluded. This point is discussed again below (Section 5.2). Whilst the model base *pressures* are not strongly affected by these uncertainties, because the rise from P_0 to P_{base} is determined by the Mg II flux, the temperature gradient would be steeper if E_m were smaller. We make no further use of

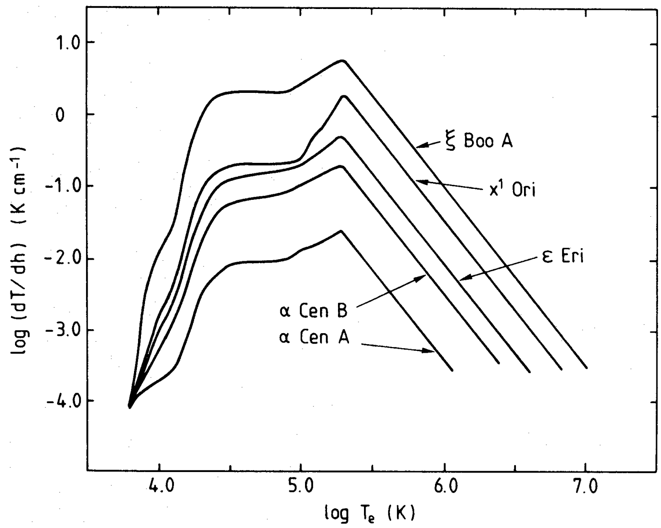

Figure 3. The temperature gradient versus temperature for the five stars. Only model b for ε Eri and model a for α Cen A are illustrated.

temperature gradients in this regime. The H Lyα flux, corrected for interstellar absorption and geocoronal emission could in principle be used to further limit E_m around $10^4-2\times10^4$ K. This is postponed to a further treatment of the whole region below 2×10^4 K.

The temperature as a function of height above a chosen base can be found by applying equations (14) or (18). Because the values of dT_e/dh cover 5 orders of magnitude the models are shown in the form of $\log(dT_e/dh)$ versus $\log T_e$ in Fig. 3. In the region above 2×10^5 K, since $P_e \simeq$ const and $E_m(T_e) \propto E_m(T_0)\, T_e^{3/2}/T_0^{3/2}$, the conductive flux is *approximately* constant and

$$\left(\frac{dT_e}{dh}\right)_{T_e} = c_1 T_e^{-5/2},$$

where $c_1 \simeq 1\times10^{-8}\, T_c^{5/2} g_*$.

Between 2×10^4 and 2×10^5 K the temperature gradient is between

$$\frac{d\ln T_e}{dh} \simeq c_2,$$

and

$$\frac{dT}{dh} = c_3$$

where the constants are $c_2 = P_e^2/E_m(0.3)\, T_e^2$ or $c_3 = P_e^2/E_m(0.3)\, T_e$. The increase in dT/dh between 6500 K and $T_e \sim 3\times10^4$ K scales as $P_0^{11/10} g_*^{1/2}$, from empirical scaling laws discussed in Section 7.

5.2 COMPARISONS WITH CHROMOSPHERIC MODELS

Models of the chromospheric below $\sim10^4$ K have been made previously for α Cen A, α Cen B, ε Eri and ξ Boo A. Models for α Cen A and B by Ayres *et al.* (1976) were based on the Ca II *K*-line and extend up to 8000 K. It is difficult to make detailed comparisons with the present results because the chromospheric models are approximate above $\sim$8000 K and ours are reliable only above $\sim 10^4$ K. However, at 8000 K both the mass column density, m, and P_T are lower in both stars by about an order of magnitude compared with the present models. Some of this difference could be caused by our overestimating the emission measure between 8000 and 2×10^4 K but because of the dominance of the first term in equation (16) the total pressure at 2×10^4 K is largely controlled by the X-ray flux and temperature, and even at 2×10^4 K our pressures are larger by factors of 2 and 5 in α Cen A and α Cen B, respectively.

Similar conclusions are reached when comparisons are made with the models calculated for ε Eri by Simon *et al.* (1980). The lines of Mg II, C II, Si II and Si III were used as well as of Ca II. Their model 2C gives a value P_T at 8000 K which is lower by a factor 4 than in our models, and this factor persists above 2×10^4 K, so that not all of the differences in pressure can be reconciled by reducing our values of E_m between 8000 and 2×10^4 K.

For ξ Boo A only a chromospheric electron density at $m=10^{-3}$ g is available for comparison (Kelch, Linsky & Worden 1979). Again the value is lower than in our models, by about a factor of 20. Overall it appears that although the method of chromospheric modelling adopted by the earlier authors, accounts for Mg II fluxes, the extension to higher temperatures tends to underestimate the transition region pressures. Further chromospheric modelling will be carried out in the future, but we note that Baliunas *et al.* (1979) found that higher pressure solutions could be made to match Ca II and Mg II profiles in other cool stars.

6 Energy balance

6.1 RADIATION LOSSES AND NET CONDUCTIVE FLUX

The radiation losses over a chosen height or temperature interval can be found by integrating

$$\frac{dF_R}{dh}=-N_e N_H P_{rad}(T_e), \tag{20}$$

where $P_{rad}(T_e)$ is the power loss (erg cm^3 s^{-1}). It is useful to consider the flux in the form

$$F_R(T_e)=\int_{h_1}^{h_2}\frac{dF_R}{dh}dh,$$
$$=\int_{h_1}^{h_2} N_e N_H P_{rad}(T_e)\, dh$$

and take h_1 to h_2 in intervals corresponding to the values of ΔR in the emission measure,

$$E'_m(0.3)=\int_{\Delta R} N_e N_H\, dh.$$

Then over ΔR,

$$\Delta F_R(T_e)\simeq E'_m(0.3)\, P_{rad}(T_e). \tag{21}$$

Several sets of calculations are used for $P_{rad}(T_e)$. Below 3×10^4 K the calculations by Hartmann & MacGregor (1980) are adopted, including their recommended scaling with gravity of $(g_*/g_\odot)^{1/4}$ from the solar values. Between 3×10^4 and 2×10^5 K we use the calculations by Summers & McWhirter (1979). Above 2×10^5 K the values are given by equation (5).

The radiation losses over a chosen temperature interval can be found by summing $\Delta F_R(T_e)$ as given in equation (21). In Table 10 the region above $\log T_e=3.75$ has been divided into intervals to show the relative importance of the radiation losses as a function of T_e and to enable

Table 10. Energy losses from radiation in different temperature ranges and energy conducted down from the corona.

Star	$F_R(T_b)$ (erg cm^{-2} s^{-1})	ΔF_R (erg cm^{-2} s^{-1})	ΔF_R (erg cm^{-2} s^{-1})	ΔF_R (erg cm^{-2} s^{-1})	ΔF_R (erg cm^{-2} s^{-1})	$F_R(T_0)$ (erg cm^{-2} s^{-1})	$F_c(T_0)$ (erg cm^{-2} s^{-1})	$F_m(T_0)$ (erg cm^{-2} s^{-1})
$\Delta \log T_e$(K)	>3.75	(3.75–3.85)	(3.85–4.35)	(4.35–5.05)	(5.05–5.35)	>5.35	>5.35	>5.35
χ^1 Ori	5.3 (7)	3.2 (7)	1.4 (7)	3.5 (6)	1.7 (5)	3.4 (6)	3.4 (7)	3.7 (7)
ξ Boo A	6.0 (7)	3.3 (7)	1.2 (7)	2.3 (6)	1.3 (5)	1.1 (7)	1.1 (8)	1.2 (8)
ε Eri (a)	2.7 (7)	2.0 (7)	7.4 (6)	1.0 (6)	6.5 (4)	3.2 (6)	3.6 (6)	6.8 (6)
(b)	2.6 (7)					2.2 (6)	9.3 (6)	1.2 (7)
α Cen A (a)	8.7 (6)	5.7 (6)	2.5 (6)	2.9 (5)	1.3 (4)	1.6 (5)	4.4 (5)	6.0 (5)
(b)	8.6 (6)					7.6 (4)	2.2 (6)	2.3 (6)
α Cen B	9.7 (6)	6.2 (6)	2.8 (6)	3.0 (5)	1.2 (4)	3.5 (5)	4.0 (6)	4.4 (6)

Notes:

ΔF_R is the energy radiated in the given temperature intervals.
$F_R(T_b)$ is the total radiation loss above $\log T_e = 3.75$.
$F_R(T_0)$ is the total radiation loss above $\log T_e = 5.35$.
$F_c(T_0)$ is the energy conducted *down* at $\log T_e = 5.3$.
$F_m(T_0)$ is the total energy loss from the region above $\log T_e = 5.3$.

comparisons to be made with heating processes. The totals above $\log T_e=3.75$ and above $\log T_e=5.30$ are also given, as $F_R(T_b)$ and $F_R(T_0)$. The intervals chosen are $\log T_e=3.75$ to 3.85, 3.85 to 4.35, 4.35 to 5.05 and 5.05 to 5.35.

The value of ΔF_R in the lowest temperature range $\log T_e=3.75$–3.85 gives a radiation loss which is larger than found by Linsky & Ayres (1978) by summing the major chromospheric line contributions. Although our emissivity for Mg II agrees to within ~20 per cent with that adopted by Linsky & Ayres the Mg II flux here is only ~12 per cent of the total, not ~30 per cent as found by Linsky & Ayres. Since we have not carried out detailed modelling of the chromosphere, we caution that our radiation losses may be overestimated there.

The major radiation loss from the 'transition region' occurs in the lower temperatures range, $\log T_e=3.85$ to 4.35. Except for ξ Boo A the energy lost between $\log T_e=4.35$ and 5.35 is comparable with the total radiation losses at temperature above $\log T_e=5.35$, which are dominated by the contribution round the coronal temperature, T_c.

The conductive flux is given by

$$F_c(T_e)=-\varkappa T_e^{5/2}\frac{dT_e}{dh}. \tag{22}$$

Using equations (14) and (15), i.e. in hydrostatic equilibrium and with $E_m(T_e)=aT_e^{3/2}$ and $\varkappa=1.1\times10^{-6}$, F_c can be re-written (Jordan 1976) as

$$F_c(T_e)=-6.2\times10^{-15}g_*(T_{\rm Top}^{5/2}-T_e^{5/2}). \tag{23}$$

$F_c(T_e)$ is an energy *loss* term down to $T_e=T_0=2\times10^5$ K, where, since $T_{\rm Top}^{5/2}=(\sqrt{2}T_c)^{5/2}\gg T_0^{5/2}$, it is given by

$$F_c(T_0)=-7.8\times10^{-7}P_0^2/a\simeq-1.4\times10^{-14}g_*T_c^{5/2}. \tag{24}$$

These values are also given in Table 10.

As in the solar atmosphere, in a static, plane-parallel atmosphere it appears to be impossible to radiate away all the energy conducted back in the layers *immediately* below T_0. Expressing $dF_c(T_e)/dT_e$ and $dF_R(T_e)/dT_e$ in terms of the emission measure $E_m(0.3)$ and using hydrostatic equilibrium one finds

$$\frac{dF_c(T_e)}{dT_e}=1.4\times10^{-8}g_*\varkappa T_e^{3/2}+\frac{\varkappa T_e^{1/2}P_e^2}{\sqrt{2}E_m(0.3)}\left[\frac{d\log E_m(0.3)}{d\log T_e}-\frac{3}{2}\right] \tag{25}$$

and

$$\frac{dF_R(T_e)}{dT_e}=0.8\sqrt{2}\frac{E_m(0.3)}{T_e}P_{\rm rad}(T_e). \tag{26}$$

Once $d\log E_m(0.3)/d\log T_e<3/2$ conduction *deposits* energy [the first term on the RHS of equation (25) is only a small loss term which becomes negligible when $b-3/2\sim10^{-2}$]. Although below $T_e\sim8\times10^4$ K the local radiation losses *can* dispose of energy deposited by conduction it is not possible to go from the region at 2×10^5 to 8×10^4 K and satisfy the constraint of $dF_R(T_e)/dT_e>dF_c(T_e)/dT_e$ with values of $E_m(0.3)$ and $d\log E_m(0.3)/d\log T_e$ which fit the observations and it is in this region that the energy carried by conduction is mainly deposited. This is a long-standing problem in the solar atmosphere (see Jordan 1980, and earlier references therein) to which there is no generally accepted solution.

Several explanations are in principle possible – mass motions may carry the energy down to layers where radiation losses are sufficient, a decreasing area factor could increase radiation losses compared with conduction, the simple treatment of conduction may be inappropriate, time varying solutions may occur, the X-ray temperature may be biased to regions of above average activity. In ξ Boo A this predicament is so extreme that, as can be seen from Table 10 the downwards conductive flux apparently exceeds the radiation loses even integrated down to Mg II. (In the solar atmosphere, similar extreme conditions exist during solar flares.)

Of the possibilities above, the effect of restricting the volume (or area) of the emitting region is the easiest one to assess. If the *coronal* emission is restricted to some cross-section area, A $(<2\pi R_*^2)$ then the mean P_c^2 derived from the X-ray flux increases by the same factor, for the same scale height. But the temperature gradient, and hence $F_c(T_0)$ remains the same, for constant A. However, because the local emission measure is increased by A, so are the radiation losses. Thus decreasing A *above* T_0 increases the local total energy flux from the corona but does not reduce the conductive flux back to the transition region. If instead the same area factor A is applied *below* T_0, then the *local* radiation losses do increase by A. To account for the apparent excess energy in χ^1 Ori and ξ Boo A in this way small area factors would be required – i.e.

$$\frac{A}{2\pi R_*^2} \sim 0.1\,(\chi^1\,\text{Ori}) \text{ and } \sim 0.02\,(\xi\,\text{Boo A}). \tag{27}$$

If such inhomogeneity were related to supergranulation structure it would *not* be revealed by rotational modulation studies. The effect on the modelling would be as follows. The electron pressure would not increase significantly because the second term in equation (16), the term including the integral of the emission measure, would still be less than P_0^2 (at 2×10^5 K). However, because E_m would increase, the temperature gradient would be less steep. If the small area factor, A, continued to the base of the model where the Mg II and C I lines are formed then, as can be seen from equation (16) the pressure would be larger by $(2\pi R_*^2/A)^{1/2}$. Further calculations of the profiles of optically thick lines formed in the chromosphere and low transition region could be used to limit the range of acceptable pressures.

Whilst clearly area factors could be important, it should be noted that in the Sun, simply allowing for the supergranulation area and flux contrast does not entirely remove the difficulties concerning the conductive flux and the anomalies may be a symptom of more fundamental energy transport problems. The main-sequence stars (see below) show systematic trends in the ratios of their X-ray, UV and chromospheric fluxes interpreted in terms of *uniform* models. To account for this behaviour including area factors requires that these also have underlying systematic trends. Meanwhile the most secure quantities are the summed radiation losses above $T_e \sim 2\times10^4$ K and above $T_0(2\times10^5$ K), which do at least provide a lower limit to the energy that is required to be deposited in these regions. Further observations of lines, for example, of O VI, formed in the region around 10^5–5×10^5 K would be of value in improving the models.

6.2 ENERGY CARRIED BY WAVE MODES

The observed full-width of half-maximum, $\Delta\lambda$, FWHM (corrected for an instrumental broadening of 25 km s^{-1}) can be used to find the rms velocity:

$$\langle V_T^2 \rangle = (3/2)\,\xi_0^2$$

where

$$\frac{\Delta\lambda}{\lambda} = 7.1\times10^{-7}\left[\frac{T_e}{M_i} + \left(\xi_0^2\frac{m_p}{2k}\right)\right]^{1/2}$$

$(M_i = M_{\text{ion}}/m_p)$.

The flux in a propagating wave is taken as

$$F_{\mathrm{wave}}=\varrho V_{\mathrm{T}}^2 V_{\mathrm{prop}}.$$

For acoustic waves

$$V_{\mathrm{prop}}=V_{\mathrm{s}}=1.5\times10^4\, T_{\mathrm{e}}^{1/2}\,\mathrm{cm\,s^{-1}}. \tag{28}$$

For MHD waves (Alfvén, or fast-mode waves where the plasma $\beta<1$),

$$V_{\mathrm{prop}}=V_A=\frac{B}{(4\pi\varrho)^{1/2}}. \tag{29}$$

Since B is not known above the photosphere, we identify the non-thermal motions with the energy removed from the field, i.e.

$$\frac{\varrho\langle V_{\mathrm{T}}^2\rangle}{2}=\frac{\langle\delta B^2\rangle}{8\pi} \tag{30}$$

and set $B^2=4\langle\delta B\rangle^2$ as a lower limit to B (Holzer, Flå & Leer 1983). The resulting values of F_{s} and F_A are given in Table 11. In a relative sense the results are similar to those found in the solar atmosphere (see Jordan, Mendoza-Ortega & Gill 1984).

In the spherically symmetric models the fluxes which could be carried by sound waves at $\sim1.3\times10^4$ K are sufficient to account for radiation losses in the range 2×10^4–10^5 K and marginally so for the total *radiation* losses above 2×10^4 K, but could *not* in all cases account also for the losses by *conduction* from the corona. Restricting the emitting area would not help. For example, assuming no dissipation until 10^5 K would require $F_{\mathrm{s}}A$=constant. With P_{e}=constant the non-thermal motions should vary as

$$V_{\mathrm{T}}^2\propto T_{\mathrm{e}}^{1/2}A^{-1}.$$

Since in all stars except α Cen B, V_{T}^2 increases more rapidly than $T_{\mathrm{e}}^{1/2}$ one could argue that A decreases between 1.3×10^4 and 10^5 K. But then the *total* energy flux available to the corona would be less. Restricting the coronal emitting area to A_{c} increases the local radiation losses by A_{c}^{-1} but raises P_0 and F_{s} by only $A_{\mathrm{c}}^{-1/2}$. One would have to invoke a geometry involving a channelling down of transition region energy fluxes into smaller coronal areas than transition region areas in order to gain from area factors – such a geometry is the contrary to what is

Table 11. Observed non-thermal motions interpreted as wave fluxes.

	Star T_{e} (K)	χ^1 Ori	ξ Boo A	ε Eri		α Cen A		α Cen B
$V_{\mathrm{T}}^{\star}$ (km s^{-1})	1.3 (4)	16	18	16		19		19
	1.0 (5)	61	47	33		35		27
				(a)	(b)	(a)	(b)	
F_{s} (erg cm^{-2} s^{-1})	1.3 (4)	6.4 (6)	2.0 (7)	3.4 (6)	3.8 (6)	8.2 (5)	8.5 (5)	1.9 (6)
	1.0 (5)	3.4 (7)	5.0 (7)	5.1 (6)	5.6 (6)	7.0 (5)	7.5 (5)	1.3 (6)
B (G)	1.3 (4)	14	25	10	10	5.0	5.0	7.6
	1.0 (5)	19	23	7.3	7.7	2.7	2.8	3.7
F_A (erg cm^{-2} s^{-1})	1.3 (4)	1.2 (7)	4.3 (7)	6.5 (6)	7.3 (6)	1.8 (6)	1.9 (6)	4.4 (6)
	1.0 (5)	8.8 (7)	9.8 (7)	7.1 (6)	7.8 (6)	1.0 (6)	1.1 (6)	1.5 (6)

$^{\star}V_{\mathrm{T}}$ from Paper I, from Si II and C IV lines, corrected for instrumental width of 25 km s^{-1}. Uncertainties are $\sim\pm15$ per cent.

observed in the solar atmosphere where the scale of structures in both the quiet and active corona is larger than corresponding transition region structures. Thus heating by acoustic waves alone, above $\sim 10^4$ K, seems unlikely, but between 10^4 and 10^5 K the total energy losses by themselves do not exclude acoustic waves. In the Sun more direct measurements of the wave flux and velocity fluctuations in the high chromosphere have been used to argue that acoustic waves are unimportant (Athay & White 1978; Bruner 1978).

There is no difficulty in providing sufficient flux with MHD waves – the Alfvén wave fluxes given in Table 11 are only lower limits taking $B^2=4\langle\delta B^2\rangle$. Although $\langle\delta B^2\rangle$ is determined by ϱV_{T}^2 quite modest increases in B above the tabulated values would suffice to account for the total energy losses.

6.3 EMISSION MEASURES PREDICTED FROM ALFVÉN WAVE HEATING

If the radiation losses between 6300 and 2×10^5 K are balanced by the dissipation of magnetic energy through Alfvén waves then the emission measure can be expressed in terms of the Alfvén wave flux and the dependence of non-thermal motions and magnetic field on temperature. The predicted emission measures can then be compared with those observed.

The observed non-thermal velocities are approximated by

$$V_{\mathrm{T}}^2=V_{\mathrm{T0}}^2\left(\frac{T_{\mathrm{e}}}{T_0}\right)^{\beta} \tag{31}$$

where the subscript 0 refers to some chosen temperature. From the available observations we know that $1\gtrsim\beta<0$, and on average $\beta\geqslant\frac{1}{2}$.

The magnetic field is expressed in terms of T_{e} rather than *assuming* a radially decreasing value, i.e.

$$B=B_0\left(\frac{T_0}{T_{\mathrm{e}}}\right)^{x} \tag{32}$$

where we know that $x>0$, since we require the field to decrease with increasing r and T.

The Alfvén wave flux is then expressed as

$$F_{\mathrm{A}}(T_{\mathrm{e}})=\left(\frac{\varrho}{4\pi}\right)^{1/2}V_{\mathrm{T0}}^2B_0\left(\frac{T_{\mathrm{e}}}{T_0}\right)^{\beta-x}. \tag{33}$$

With $P_{\mathrm{e}}=$const, tenable down to 2×10^4 K for these stars,

$$F_A(T_{\mathrm{e}})=F_A(T_0)\left(\frac{T_{\mathrm{e}}}{\mathrm{T}_0}\right)^{\beta-x-1/2}$$

and

$$\frac{dF_A(T_{\mathrm{e}})}{dT_{\mathrm{e}}}=F_A(T_0)(\beta-x-\tfrac{1}{2})\left(\frac{T_{\mathrm{e}}}{T_0}\right)^{\beta-x-1/2}T_{\mathrm{e}}^{-1}.$$

Now, recalling that the radiation losses can be expressed in terms of the emission measure,

$$\frac{dF_{\mathrm{R}}(T_{\mathrm{e}})}{dT_{\mathrm{e}}}=0.8\sqrt{2}P_{\mathrm{rad}}(T_{\mathrm{e}})\,E_{\mathrm{m}}(0.3)\,T_{\mathrm{e}}^{-1}.$$

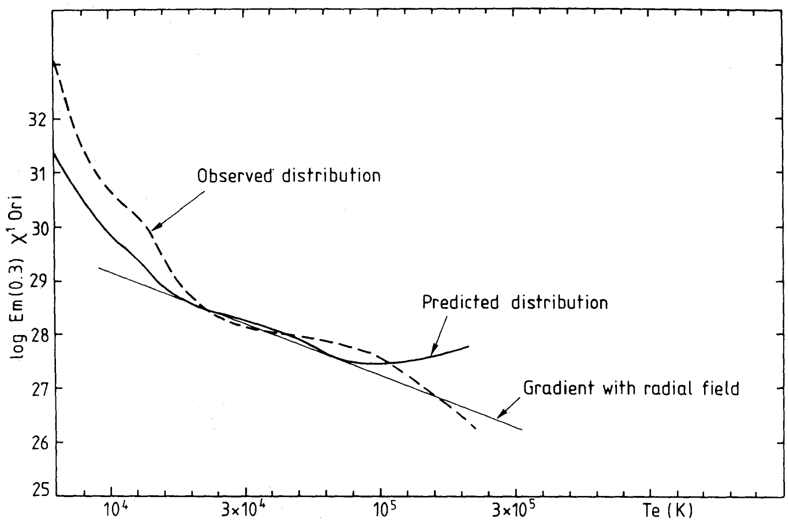

Figure 4. The computed emission measure for χ^1 Ori based on energy derived from Alfvén waves, compared with the observed mean distribution. The curves are normalized at 10^5 K. The gradient expected with a radial magnetic field is also shown.

Balancing $dF_A(T_e)/dT_e$ against $-dF_R(T_e)/dT_e$ then yields

$$E_m(0.3) = -\frac{F_A(T_0)}{0.8\sqrt{2}}\,\frac{(\beta - x - \tfrac{1}{2})}{P_{rad}(T_e)} \times \left(\frac{T_e}{T_0}\right)^{\beta - x - 1/2}. \tag{34}$$

Since the heating flux must decrease with increasing T_e and $E_m(0.3)$ must be positive, we require $\beta - x - \tfrac{1}{2} < 0$.

Suppose the reference point is chosen as $T_0 = 2\times10^5$ K. Then we require a value of $F_A(T_0)$ that will account for the total losses frm the corona above, i.e. $F_A(T_0) = F_m(T_0)$ as given in Table 10. Adopting $P_{rad}(T_e)$ from Hartmann & MacGregor (1980), the value of $(\beta - x - \tfrac{1}{2})$ required to bring the observed and calculated values of $E_m(0.3)$ into agreement at C IV (10^5 K) can be found. For χ^1 Ori (used as a test case) this value is small, i.e. $\beta - x - \tfrac{1}{2} = -0.05$.

This implies that $F_A(T_e)$ decreases slowly with T_e, i.e. very little local heating is required. Also the *form* of the emission measure distribution below $T_e \sim 2\times10^5$ K is then determined primarily by the form of the radiative power loss distribution. The computed distribution is shown in Fig. 4, with the mean distribution derived from the observations of χ^1 Ori. Between 10^5 and 2×10^5 K conduction will still be important so the form of E_m there will not be accurate. Below 10^4 K the simple approximation for the pressure will fail and also there are uncertainties in both $P_{rad}(T_e)$ and the observed distribution. As mentioned above the observed distribution could be too high between 10^4 K and 2×10^4 K with Si II and C II being formed at slightly lower and higher temperatures, respectively. However, the observed and calculated distributions agree remarkably well.

The formulation also predicts that the emission measure at $\sim10^5$ K should scale as $F_m(T_0)$ if $(\beta - x - \tfrac{1}{2})$ has the same value in the different stars. This is acceptable except for ξ Boo A which is usually anomalous in the scaling laws discussed in the next section.

The limits on β and x above show immediately that $\beta > 0.45$ and $x < 0.55$. To determine the individual values of β and x a further assumption is required. We have adopted above

$$\varrho V_T^2 = \left\langle \frac{\delta B^2}{4\pi} \right\rangle, \tag{35}$$

identifying the non-thermal motions with energy removed from the magnetic field. We now assume that

$$dB(T_e) \propto \langle \delta B^2 \rangle^{1/2}$$

which leads to $\beta = 1 - 2x$. The individual values of β and x are then $\beta = 0.63$ and $x = 0.18$. Whilst not wishing to place too much emphasis on precise numbers it is of interest to note that with a radial magnetic field

$$B(r) = B_0 \left(\frac{r_0}{r} \right)^2$$

and $x = 0.18$ the emission measure is predicted to decrease according to

$$E_m(T_e) \propto T_e^{-1.9}.$$

This gradient is shown in Fig. 4 and is in good agreement with that observed over the temperature range of most interest. We have not assumed above any method of dissipating the Alfvén waves – the damping lengths implied are shorter than could be accounted for by known methods in a linear treatment. As a rough average, the local damping length required is only $\sim 10^{-2}$ of the local isothermal pressure scale height, whatever type of wave is considered. The damping of Alfvén waves remains a theoretical problem deserving further attention.

The same analysis can be carried out for acoustic waves, where only β enters as the unknown temperature dependence (equation 31). It is obvious that if one requires acoustic waves to balance the *same* energy flux above T_0 then for the same emission measure, $(\beta - ½) = -0.05$ – i.e. the *same* functional form of $E_m(0.3)$ results. But the value of β is now $\beta \sim 0.45$ and not $\beta \sim 0.63$ (see below), as in the case of Alfvén waves. If acoustic waves were the source of heating, for example, through shock dissipation, then very short-period waves ($\tau \leq 10$ s) would be required (see Athay 1976). Improved measurements of the variation of linewidths with temperature, for example with the *Hubble Space Telescope* offer the best hope of eventually distinguishing between wave modes.

7 Comparison with scaling laws

A number of scaling laws between chromospheric, transition region and coronal fluxes, rotation rates and stellar convective zone parameters have been discussed in the literature in attempts to establish the factors that control coronal conditions. Scaling laws between coronal parameters have also been predicted on the basis of simple models, e.g. the minimum energy loss concept (or maximum pressure solution) of Hearn (1975, 1977) or the loop model by Rosner, Tucker & Vaiana (1978). Here we make comparisons between the observations, our models and the predictions of scaling laws.

7.1 CORONAL PARAMETER SCALING LAWS

Hearn (1975, 1977) proposed scaling laws based on the concept of a corona relaxing to a minimum energy loss configuration. His method implies that there is a fixed ratio between the radiation losses and conductive flux from the corona and with $P_{rad}(T_e) \propto T_e^{-1/2}$ the scaling laws become

$$P_* = 3 \times 10^{-18} g_* T_*^2 \tag{36}$$

and

$$E_m(T_*) = 3.3 \times 10^4 T_*^3 g_*, \tag{37}$$

where P_* is the *electron* pressure (in dyne cm^{-2}) at the base of the corona. Identical scaling laws result from adapting closed loop models with constant pressure (e.g. Rosner *et al.* 1978) to apply to an open atmosphere by replacing L, the loop length by $H/2$ where H is the isothermal scale height. This approach has been discussed by Schrijver *et al.* (1984). The data they display for dwarf stars are consistent with $E_m(T_c) \propto T_c^3 g_*$, as are data given by Landini, Monsignori-Fossi & Pallavicini (1986).

The same scaling laws can be derived from the more general relations discussed in Section (6) (Jordan 1980), i.e. since

$$F_R(T_0) \propto E_m(T_c)\ T_c^{-1/2}$$

and

$$|F_c(T_0)| \propto \left(\frac{dT}{dh}\right)_{T_0} \propto \frac{P_0^2}{E_m(T_0)}$$

then with

$$E_m(T_c) = E_m(T_0)\left(\frac{T_c}{T_0}\right)^b \quad \text{and} \quad F_R(T_0) \propto |F_c(T_0)|$$

one derives

$$E_m(T_c) \propto P_0 T_c^{(b+1/2)/2}.$$

But also

$$E_m(T_c) \propto \frac{P_c^2}{T_c}\frac{1}{g_*}$$

and

$$P_c^2 \propto P_0^2.$$

Hence assuming $F_R(T_0) \propto |F_c(T_0)|$ yields $P_0 \propto T_c^{(b+5/2)/2} g_*$. With $b=3/2$ this gives

$$P_0 \propto T_c^2 g_*$$

as before, in equation (36).

The *observed* X-ray flux, as discussed in Section (3), scales as $F_X \propto E_m(T_c)\,P_{\rm rad}(T_c) f(T_c) \propto E_m(T_c)$ which gives $F_X \propto T_c^3 g_*$.

In general, the *total* radiation loss and conductive flux at T_0 scale as

$$\left.\begin{aligned} &F_R(T_0) \propto P_c^2 g_*^{-1}\ T_c^{-3/2} \propto P_c^{5/4}\ g_*^{-1/4} \\ &\text{and} \\ &|F_c(T_0)| \propto g_*\ T_c^{b+1} \propto P_c^{5/4} g_*^{-1/4} \end{aligned}\right\} \qquad (38)$$

and similarly

$$F_m(T_0) = F_R(T_0) + F_c(T_0) \propto P_c^{5/4} g_*^{-1/4}. \qquad (39)$$

Fig. 5(a) and (b) give a comparison between the values of P_c and $E_m(T_c)$ derived from the observed X-ray fluxes and temperatures and the predictions of Hearn's method, from equations (36) and (37), identifying T_* with T_c. It can be seen that the observed pressures are consistent with the powers in the scaling law (a spread of $\sim \pm 0.10$ about the log of the mean), but are

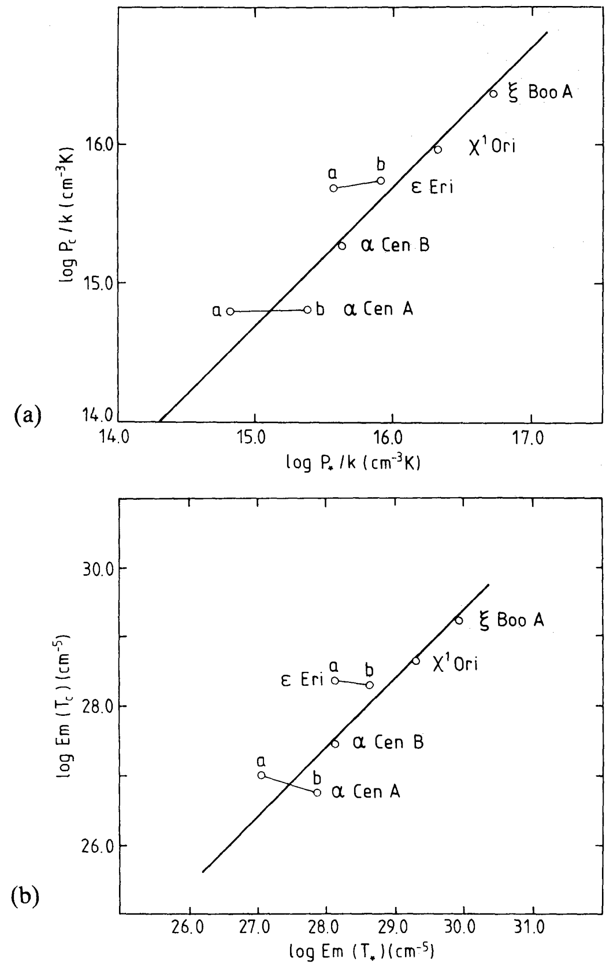

Figure 5. (a) Comparison of average coronal pressure with predictions of Hearn's minimum energy loss hypothesis. (b) Comparison of coronal emission measures with predictions of Hearn's minimum energy loss hypothesis.

systematically a factor of 2.0 lower. Similarly, the observed emission measures scale according to the predicted powers, but are a factor of 4.0 lower. The higher temperature solution for ε Eri seems more appropriate. The total energy losses agree well because the conductive flux dominates. A small systematic difference in the observed and predicted values of P_c is not surprising since we identify P_c with P_* in Hearn's formulation. However, the powers in the scaling laws are determined by dimensional arguments and that the underlying (detailed) physics is contained in the numerical constants. The empirically adjusted relations,

$$P_c = 1.5\times10^{-18} g_* T_c^2 \tag{40}$$

and

$$E_m(T_c) = 8.2\times10^3 g_* T_c^3 \tag{41}$$

account remarkably well for the observations. These give a larger ratio of $F_c(T_0)/F_R(T_0)$ than in the minimum energy loss method.

7.2 LOOP SCALING LAWS

The scaling law between loop pressure, P_0, maximum temperature, T_c and loop length, L, in a constant pressure model, proposed by Rosner *et al.* (1978) also implies a fixed ratio between the radiative and conductive fluxes from the loop. The scaling (not necessarily the constants) can be seen simply by setting $F_R(T_0) \propto F_c(T_c)$ as above. Then

$$0.8\, E_m(T_c)\, P_{rad} \propto \varkappa T_c^{5/2} \frac{dT}{dh}.$$

In the simple loop model dT/dh is replaced by $T_c L^{-1}$ and $E_m(T_c)$ by $\overline{N_c^2 L}$. Thus with

$$P_{rad} \propto T_c^{-1/2},$$

one finds

$$P_c L \propto T_c^3.$$

The numerical relationship found by Rosner *et al.* is

$$T_{max} \propto 1.4 \times 10^3 (1.8\, P_c L)^{1/3}. \tag{42}$$

As pointed out by Hearn & Kuin (1981) replacing $H/2$ by L in Hearn's approach leads to the same relation. The difficulty with the loop approach is that it introduces a further unknown quantity, L. In the hydrostatic model L is the isothermal scale height, determined by the measured T_c and g_*, and thus P_c can be found from the emission measure. Also, if a loop is postulated the cross-section area A, or 'filling factor' $f = A/4\pi R_*^2$ must be introduced as a further unknown factor. Then only the quantity

$$P_c f = 4.9 \times 10^9 \frac{E_m(T_c)}{T_{max}} \tag{43}$$

can be found – where $E_m(T_c)$ is calculated with spherical symmetry. The parameter space L as a function of f can be explored. Recognizing that the loops can be larger than the isothermal scale height and thus constant pressure is a poor approximation, some authors have added a further exponential hydrostatic term (e.g. Serio *et al.* 1981). This is unnecessary since replacing L by $H/2$ allows for hydrostatic equilibrium.

The loop scaling laws have been applied by other authors to some of the stars considered here, but since the observations do not determine L or f, the solutions found must depend on other assumptions made, for example a heating function and base boundary conditions. Giampapa *et al.* (1985) have modelled ε Eri and α Cen B in terms of loop structures, including the hydrostatic term proposed by Serio *et al.* (1981). The loop cross-sectional area is taken as constant, all loops are assumed to be identical and a uniform heating (per unit volume) is assumed.

The filling factor is found by satisfying both UV and X-ray fluxes. This procedure, plus the requirement for the conductive flux to tend to zero smoothly at the base must effectively *determine* the form of the emission measure distribution between 10^5 K and the corona. The authors themselves point out that for α Cen B the best-fit models do not satisfy all the radiative diagnostics and for ε Eri the models show a systematic overprediction of UV fluxes. For α Cen B, with $T_c = 2.4 \times 10^6$ K they find $P_e = 0.31$ dyne cm^{-2}, $f = 1.68$ and $L = 90.5 \times 10^9$ cm. This pressure is similar to the one we derive because $f \sim 1$, although $f > 1.0$ is not physical, i.e. the model is not significantly different from the spherically symmetric case. For ε Eri with $T_c = 3.5 \times 10^6$ K they derive $P_e \sim 2.5$–10 dyne cm^{-2}, for $f \sim 0.54$–0.22 and $L \sim 7.5 \times 10^8$–3.0×10^9 cm. Again, as we would expect a model with $f = 0.54$ has a pressure only a factor ~ 3 larger than the one we derive, but a loop length $\ll H/2$ is surprising if long-term structures exist in the corona. Studies of X-ray variability including rotational modulation are needed to distinguish between the 'average' corona and the effects of active regions.

Landini *et al.* (1985) have used α Cen A as an example for general calculations of expected

EUV emission from stars. They make hydrostatic models for loops with constant filling factor but also constrain the solutions by adopting a uniform heating function and a conductive flux tending to zero at 2×10^4 K. The filling factor is found by selecting a value of P_0/P_c; two models corresponding to (i) $P_0/P_c=1.1$ and (ii) $P_0/P_c=e$ are made. In our formation $P_0/P_c=1.1$ and hydrostatic equilibrium implies an emission measure $E_m \propto T_e^{3/2}$ between 2×10^5 K and T_c. However, for model 1 they find $P_0/k \sim 2\times10^{16}\,\mathrm{cm}^{-3}$ K, $T_c=2.5\times10^6$ K, $L=2.8\times10^9$ cm and $f=0.015$ (their table 3 contains a misprint of $f=0.15$). Such a high pressure is not consistent with the density constraints from Si III] and the mean emission measure around $3-6\times10^4$ K. Model 2 has $P_0/k=4.4\times10^{15}\,\mathrm{cm}^{-3}$ K, similar to our upper limit but $T_c=3.8\times10^6$ K, $L=4.4\times10^{10}$ cm and $f=0.056$. More accurate line fluxes for density sensitive lines and a separate determination of the temperature of the X-ray emitting region in α Cen A are required to further limit the range of solutions.

7.3 FLUX CORRELATIONS

The correlations between chromospheric, transition region and coronal fluxes have been investigated by a number of authors. The trend for coronal fluxes and transition region fluxes to depend on some power, greater than unity, of the Mg II flux has been established for some years (e.g. Ayres *et al.* 1981; Hartmann, Dupree & Raymond 1982).

Ayres *et al.* (1981), proposed the following relations,

$$\frac{F_X}{F_{\mathrm{bol}}} \propto \left(\frac{F_{\mathrm{Mg\,II}}}{F_{\mathrm{bol}}}\right)^3$$

and

$$\frac{F_{\mathrm{Tr}}}{F_{\mathrm{bol}}} \propto \left(\frac{F_{\mathrm{Mg\,II}}}{F_{\mathrm{bol}}}\right)^{3/2} \tag{44}$$

[$F_{\mathrm{Tr}}=F(\mathrm{Si\,IV}+\mathrm{C\,IV}+\mathrm{N\,V})$, but $F(\mathrm{C\,IV})$ dominates the total]. A comprehensive survey by Oranje (1986) has resulted in a similar scaling law, i.e.

$$F_{\mathrm{Tr}} \propto F_{\mathrm{Mg\,II}}^{1.57}. \tag{45}$$

He also finds that C II (1335 Å) correlates well with C IV (1550 Å) in spite of its low temperature of formation ($\sim 2\times10^4$ K). For the stars considered here it can be shown from the data given in the tables that the relation

$$F_{\mathrm{Tr}} \propto F_{\mathrm{Mg\,II}}^{3/2} \tag{46}$$

holds more precisely than do the relations between F_X and $F_{\mathrm{Mg\,II}}$ or F_X and F_{Tr} and only this relation will be adopted in Section 7.4.

The dependence of the Mg II flux on stellar properties, such as T_{eff} and g_* has also been examined. The results of various authors (e.g. Linsky & Ayres 1978; Basri & Linsky 1979; Kelch *et al.* 1979; Weiler & Oergerle 1979; Stencel *et al.* 1980), can be summarized as

$$\frac{F_{\mathrm{Mg\,II}}}{T_{\mathrm{eff}}^4} \propto T_{\mathrm{eff}}^{2\pm2}\frac{1}{g_*^{1/4}}. \tag{47}$$

This scaling is similar to that predicted for the flux carried by an acoustic slow mode of Alfvén mode when the magnetic field is weak or has an equipartition value (Stein 1981), although it is not known how the non-thermal flux is modified between the photosphere and high chromosphere

(Ulmschneider & Stein 1982). However, the five stars considered here fit relation (34) only to within a factor of ± 0.3 dex about the mean. Relations involving $T_{\rm eff}$ are difficult to establish for cool stars because of the small range of values involved. For example, both relations (31) and (32) give satisfactory fits (within ± 0.10 about the log of the mean) in spite of a difference of $T_{\rm eff}^2$. Although the convective zone properties are built into the scaling laws found by Stein and the magnetic field is scaled according to the gas pressure, the rotation rate is not explicitly involved.

Whilst exploring correlations between $F_{\rm Mg\,II}$ and F_X and $F_{\rm Tr}$ and the model parameters, we found that $P_e P_H$, derived from the Mg II flux and scale height or from integrating the emission measure distribution, correlates with P_0, the model transition pressure, according to $P_e P_H \propto P_0^{3/5}$, which implies

$$F_{\rm Mg\,II} \propto \frac{P_e P_H}{g_*} \propto \frac{P_0^{3/5}}{g_*}. \tag{48}$$

This relation is combined below with coronal scaling laws (see Section 7.2). Since for these stars P_H does not vary greatly, the scaling mainly reflects a relationship between P_e around 6500 K and P_0. The electron pressure is not the main contributor to the total pressure but reflects the atomic processes controlling the degree of ionization below $\sim 2\times 10^4$ K. In our models this is dealt with in a very simple approximation but more detailed chromospheric modelling may show how this scaling with P_e arises.

7.4 COMBINATION OF FLUX RELATIONS AND CORONAL SCALING LAWS

In Section 7.2, we have shown that the scaling between coronal pressure, temperature and stellar gravity which arises from a constant ratio between $F_R(T_0)$ and $F_c(T_0)$ gives an acceptable fit to the observed parameters, i.e.

$$P_c \propto P_0 \propto T_c^2 g_*.$$

Substituting this scaling into the expression for the X-ray flux leads to $F_X \propto T_c^3 g_* \propto P_0^{3/2} g_*^{-1/2}$.

Also, the flux relation

$$F_{\rm Tr} \propto F_{\rm Mg\,II}^{3/2}. \tag{49}$$

which holds well for these stars is adopted.

The third starting relation is the empirical one,

$$F_{\rm Mg\,II} \propto P_0^{3/5} g_*^{-1}.$$

The transition region flux can be written as

$$F_{\rm Tr} \propto P_0^2 \left(\frac{dh}{dT}\right)_{10^5\,\rm K}. \tag{50}$$

Relations (48), (49) and (50) can then be combined to show

$$\left(\frac{dT}{dh}\right)_{10^5\,\rm K} \propto P_0^{11/10} g_*^{3/2}$$

and hence

$$F_{\rm Tr} \propto P_0^{9/10} g_*^{-3/2}. \tag{51}$$

The relations which then result between F_X, F_{Tr} and $F_{\mathrm{Mg\,II}}$ are

$$F_X \propto F_{\mathrm{Tr}}^{5/3} g_*^2 \tag{52}$$

and

$$F_X \propto F_{\mathrm{Mg\,II}}^{5/2} g_*^2 \tag{53}$$

i.e. the powers of F_{Tr} and $F_{\mathrm{Mg\,II}}$ are somewhat lower than the values of 2 and 3 in the relations (44) which involve F_{bol}. It can be shown that the higher powers of relation (44) *would* result if we started from

$$P_e P_H \propto P_0^{1/2}.$$

Then

$$F_X \propto F_{\mathrm{Tr}}^2 g_*^{5/2}$$

and

$$F_X \propto F_{\mathrm{Mg\,II}}^3 g_*^{5/2}. \tag{54}$$

Although the relation $P_e P_H \propto P_0^{3/5}$ fits the data better than $P_e P_H \propto P_0^{1/2}$ there is little to choose between relations (52, 53) and (54) when F_X, F_{Tr}, $F_{\mathrm{Mg\,II}}$ and g_* are compared directly. A larger data set could eventually distinguish between these relations but we note that a combination of the data from Oranje (1986) and Schrijver *et al.* (1984) does suggest that the relation $F_X \propto F_{\mathrm{Tr}}^{5/3}$ might be more appropriate than $F_X \propto F_{\mathrm{Tr}}^2$.

7.5 CORRELATIONS WITH ROTATION PERIOD

Given the spread of L_X or F_X at a particular T_{eff} and the expected role of the sub-photospheric convection zone generating magnetic fields, a number of authors have explored correlations with the rotation rate ($v \sin i$ or P-period) and the effective Rossby number which reflects convective zone conditions (e.g. Ayres *et al.* 1981; Pallavicini *et al.* 1981; Noyes *et al.* 1984; Hartmann *et al.* 1984). Similarly, Simon, Herbig & Boesgaard (1985) have investigated the dependence of fluxes on rotation rates and convective turnover times.

Mangeney & Praderie (1984) have found a correlation between the X-ray flux, F_X, normalized to the flux F_c, the kinetic energy flux in the region of maximum convective velocity, and the effective Rossby number, R_0^*, such that

$$\frac{F_X}{F_c} \propto (R_0^*)^{-3.3}. \tag{55}$$

R_0^* is defined as

$$R_0^* = \frac{1}{2} \frac{V_m}{\Omega L_c}$$

where V_m is the maximum convective velocity, L_c is the depth of the convective zone and Ω is the rotation rate. Alternatively,

$$R_0^* = \frac{V^*}{V_{\mathrm{eq}} \sin i}$$

where V_{eq} is the equatorial rotational velocity and

$$V^* = ½ \frac{V_m R_*}{L_c}.$$

From table 1 of Mangeney & Praderie (1984) it appears that $\log F_c = \text{const} = 10.05 \pm 0.05$ for main-sequence stars cooler than G0. Also, for stars of mass $M \leq M_\odot$ the velocity $V^* \propto T_{\text{eff}}^4$. Thus, for the stars considered here

$$R_0^* \propto \frac{T_{\text{eff}}^4}{V_{\text{eq}} \sin i}$$

and

$$F_X \propto \left(\frac{V_{\text{eq}} \sin i}{T_{\text{eff}}^4} \right)^{3.3} \tag{56}$$

since $V_{\text{eq}} \sin i \propto R_*/P$, where P is the period of rotation, and for cool main-sequence stars, $R_* \propto T_{\text{eff}}$, the flux/period relation becomes

$$F_X \propto P^{-3.3} (T_{\text{eff}}^3)^{-3.3} \tag{57}$$

Marilli & Catalano (1984) find

$$L_X \propto P^{-3} \tag{58}$$

but also could fit with an exponential law. Similarly Walter (1982) prefers an exponential dependence $\log L_X \propto P^{-n}$ but points out that a fit with two power laws, $P^{-1.21}$, $P^{-3.83}$ with a break at ~10 days could also be justified.

Regarding other luminosities, the data presented by Marilli & Catalano (1984) for $L_{\text{C IV}}$ fit a power law,

$$L_{\text{C IV}} \propto P^{-1.86},$$

or

$$F_{\text{C IV}} \propto P^{-1.8} T_{\text{eff}}^{-1}.$$

Schrijver *et al.* (1984) make a two-parameter fit to X-ray emission measures, and find

$$F_X \propto E_m(T_c) \propto T_c^{1.51} P^{-0.88}.$$

It is clear that the flux, luminosity and rotation correlations cannot *all* be fitted together in a mutually consistent manner, and further work on correlations with larger data sets and improved stellar parameters are required.

Here we explore the consequences of combining the relation

$$F_X \propto P^{-3} T_{\text{eff}}^n \tag{59}$$

($n \sim -2$ to -9.9) with the coronal scaling laws

$$F_X \propto g_* T_c^3 \propto P_0^{3/2} g_*^{-1/2}.$$

These give

$$P_0 \propto g_*^{1/3} P^{-2} T_{\text{eff}}^{2n/3} \tag{60}$$

and

$$T_c \propto g_*^{-1/3} P^{-1} T_{\text{eff}}^{n/3} \tag{61}$$

i.e. the 'activity' as measured by either T_c or P_0 increases with shorter periods, as expected.

If one is prepared to use the simple dimensional arguments below, the magnetic field can also be related to P_0, T_c and P. Suppose that the corona derives its energy from the magnetic field, with an energy flux

$$F_m \propto \frac{\langle \delta B^2 \rangle}{4\pi} V_A \propto \frac{\langle \delta B^2 \rangle}{B^2} \frac{B^3}{\varrho^{1/2}} \tag{62}$$

reaching the corona. If the same dissipation process is ubiquitous then one might expect $\langle \delta B^2 \rangle / B^2 \sim$constant. Then if F_m is proportional to the energy losses, F_R or F_c, one has

$$B^3 T_c^{1/2} P_0^{-1/2} \propto P_0^2 T_c^{-3/2} g_*^{-1}. \tag{63}$$

But, as discussed above,

$$P_0 \propto T_c^2 g_*, \qquad \text{leading to } B^2 \propto P_0, \tag{64}$$

as one might expect since dimensional arguments have been applied, and

$$B \propto T_c g_*^{1/2}. \tag{65}$$

The same results can be found by arguing that the thermal energy density of the corona is maintained by a wave propagating at V_A, i.e.

$$F_m \propto P_0^{1/2} B T_0^{1/2}.$$

With $F_m \propto F_R \propto F_c$ this again leads to $B^2 \propto P_0$.

In terms of the rotational period, P, this gives

$$B \propto P^{-1} g_*^{1/6} T_{\rm eff}^{n/3} \tag{66}$$

i.e. the coronal field is controlled by the rotation rate.

The X-ray, transition region and chromospheric fluxes can then be found simply in terms of B and g_*, i.e. from (48), (49), and (52), with $P_0 \propto B^2$,

$$F_X \propto B^{5/2} g_*^{-1/4} \; F_{\rm Tr} \propto B^{9/5} g_*^{-3/2}$$

and

$$F_{\rm Mg\,II} \propto B^{6/5} g_*^{-1}.$$

The dependence of the C IV and Mg II fluxes on period which follow from

$$F_X \propto P^{-3} T_{\rm eff}^n$$

are then

$$F_{\rm Tr} \propto P^{-1.8} g_*^{-6/5} T_{\rm eff}^{3n/5} \tag{67}$$

and

$$F_{\rm Mg\,II} \propto P^{-1.2} g_*^{-4/5} T_{\rm eff}^{2n/5}. \tag{68}$$

These relations agree well with the data presented by Marilli & Catalano (1984) and by Simon *et al.* (1985).

8 Conclusions

Models of the chromospheric–coronal transition regions and coronae have been made for a sample of main-sequence stars by combining UV and X-ray observations. The surface fluxes above the chromosphere correlate with the coronal pressure and temperature, whose values range from being similar to those in the 'quiet' solar atmosphere to values typical of a well-developed active region. Whilst time-dependent UV and X-ray observations are required to establish the effects of inhomogeneous structures the present modelling in terms of spherically symmetric atmospheres does not show any obvious inconsistencies.

The form of the emission measure distributions between $T_e \sim 2\times10^4$ and 10^5 K can be accounted for if the non-thermal line broadening is assumed to represent energy deposited by the passage of Alfvén (or fast-mode) waves, and this is balanced by local radiation losses. Improved observations of line profiles at higher spectral resolution are required to test the hypothesis.

The coronal pressures and temperatures fit correlations expected from dimensional arguments, but the physics controlling this behaviour enters into the constant of proportionality.

Flux and rotation correlations from the literature have been combined with coronal parameter scaling laws to predict the dependence of the coronal pressure and temperature on rotation rates; these could be tested against a wider sample of data. The correlations *between* transition region and X-ray fluxes can be understood in terms of pressure correlations arising from the process producing the emission, but the correlation between chromospheric and coronal fluxes remains empirical. Further work on the structure and energy balance of the chromosphere–transition region interface would be particularly useful.

Although global properties can be explored through dimensional arguments the theory of the dependence of coronal properties on specific energy propagation and dissipation mechanisms remains at an early stage but the more detailed observations possible in the solar atmosphere offer some hope of progress.

Acknowlegments

CJ is grateful for support from the UK SERC for *IUE* observing. The work of AB, JLL and TRA was supported by NASA grant NAG 06–003–057 and NAG 5-82 to the University of Colorado. TS was supported by NASA grant NAG 5-11-6 to the University of Hawaii.

The *IUE* spectra used were obtained at both VILSPA, Madrid and Goddard Space Flight Center and we are grateful to the staff at both ground stations for their support.

References

Athay, R. G., 1976. *The Solar Chromosphere and Corona: Quiet Sun*, p. 490, Reidel, Dordrecht, Holland.
Athay, R. G. & White, D. R., 1978. *Astrophys. J.*, **226**, 1135.
Ayres, T. R. & Linsky, J. L., 1980. *Astrophys. J.*, **235**, 76.
Ayres, T. R., Marstad, N. C. & Linsky, J. L., 1981. *Astrophys. J.*, **247**, 545.
Ayres, T. R., Linsky, J. L., Rodgers, A. W. & Kurucz, R. L., 1976. *Astrophys. J.*, **210**, 199.
Ayres, T. R., Linsky, J. L., Simon, T., Jordan, C. & Brown, A., 1983. *Astrophys. J.*, **274**, 784.
Ayres, T. R., Linsky, J. L., Basri, G. S., Landsman, W., Henry, R. C., Moos, H. W. & Stencel, R. E., 1982. *Astrophys. J.*, **256**, 550.
Baliunas, S. L. & Butler, S. E., 1980. *Astrophys. J.*, **235**, L45.
Baliunas, S. L., Avrett, E. H., Hartmann, L. & Dupree, A. K., 1979. *Astrophys. J.*, **233**, L139.
Basri, G. S. & Linsky, J. L., 1979. *Astrophys. J.*, **234**, 1023.
Boesgaard, A. M. & Simon, T., 1984. *Astrophys. J.*, **277**, 241.
Borra, E. F., Edwards, G. & Mayor, M., 1984. *Astrophys. J.*, **284**, 211.
Brown, A., Ferraz, M. C. de M. & Jordan, C., 1984. *Mon. Not. R. astr. Soc.*, **207**, 831.
Brown, A., Jordan, C., Stencel, R. E., Linsky, J. L. & Ayres, T. R., 1984. *Astrophys. J.*, **283**, 731.
Bruner, E., 1978. *Astrophys. J.*, **226**, 1140.
Demarque, P., Guenther, D. B. & Van Altena, W. F., 1986. *Astrophys. J.*, **300**, 773.
Dufton, P. L. & Kingston, A. E., 1985. *Astrophys. J.*, **289**, 844.
Dufton, P. L., Hibbert, A., Kingston, A. E. & Doschek, G. A., 1983. *Astrophys. J.*, **274**, 420.

Flannery, B. P. & Ayres, T. R., 1978. *Astrophys. J.*, **221**, 175.
Giampapa, M. S., 1984. In: *Stellar Activity and Variability*, p. 309, eds Mangeney, A. & Praderie, F., Meudon.
Giampapa, M. S., Golub, L., Peres, G., Serio, S. & Vaiana, G. S., 1985. *Astrophys. J.*, **289**, 203.
Golub, L., Harnden, F. R. Jr, Pallavicini, R., Rosner, R. & Vaiana, G. S., 1982. *Astrophys. J.*, **253**, 242.
Gondoin, Ph., Giampapa, M. S. & Bookbinder, J. A., 1985. *Astrophys. J.*, **297**, 710.
Guenther, D. B. & Demarque, P., 1986. *Astrophys. J.*, **301**, 207.
Hartmann, L. & MacGregor, K. B., 1980. *Astrophys. J.*, **242**, 260.
Hartmann, L., Dupree, A. K. & Raymond, J. C., 1982. *Astrophys. J.*, **252**, 214.
Hartmann, L., Baliunas, S. L., Duncan, D. K. & Noyes, R. W., 1984. *Astrophys. J.*, **279**, 778.
Hartmann, L., Jordan, C., Brown, A. & Dupree, A. K., 1985. *Astrophys. J.*, **296**, 576.
Hearn, A. G., 1975. *Astr. Astrophys.*, **40**, 355.
Hearn, A. G., 1977. *Sol. Phys.*, **51**, 159.
Hearn, A. G. & Kuin, N. P. M., 1981. *Astr. Astrophys.*, **98**, 248.
Hoffleit, D., 1964. *Catalogue of Bright Stars*, Yale University, New Haven.
Holtzer, T. E., Flå, T. & Leer, E., 1983. *Astrophys. J.*, **275**, 808.
Johnson, H. M., 1981. *Astrophys. J.*, **243**, 234.
Jordan, C., 1967. *Sol. Phys.*, **2**, 441.
Jordan, C., 1969a. *Astrophys. J.*, **156**, 49.
Jordan, C., 1969b. *Mon. Not. R. astr. Soc.*, **142**, 501.
Jordan, C., 1976. *Phil. Trans. R. Soc. London*, **A281**, 391.
Jordan, C., 1980. *Astr. Astrophys.*, **86**, 355.
Jordan, C. & Brown, A., 1981. In: *Solar Phenomena in Stars and Stellar Systems*, p. 199, eds Bonnet, R. M. & Dupree, A. K., Reidel, Dordrecht, Holland, NATO ASIC, 68.
Jordan, C., Mendoza-Ortega, B. E. M. & Gill, R. S., 1986. *Proc. 4th European Meeting on Solar Physics, The Hydromagnetics of the Sun, ESA SP-220*, p. 138.
Kamper, K. W. & Wesselink, A. J., 1978. *Astr. J.*, **83**, 1633.
Kato, T., 1976. *Astrophys. J. Suppl.*, **30**, 397.
Kelch, W. L., 1978. *Astrophys. J.*, **222**, 931.
Kelch, W. L., Linsky, J. L. & Worden, S. P., 1979. *Astrophys. J.*, **229**, 700.
Landini, M., Monsignori-Fossi, B. C. & Pallavicini, R., 1986. In: *Proc. X-ray Astronomy, 1984*, p. 83, Bologno University.
Landini, M., Monsignori-Fossi, B. C., Paresce, F. & Stern, R. A., 1985. *Astrophys. J.*, **289**, 709.
Linsky, J. L., 1985. *Sol. Phys.*, **100**, 333.
Linsky, J. L. & Ayres, T. R., 1978. *Astrophys. J.*, **220**, 619.
Mangeney, A. & Praderie, F., 1984. *Astr. Astrophys.*, **130**, 143.
Marcy, G. W., 1981. *Astrophys. J.*, **245**, 624.
Marcy, G. W., 1984. *Astrophys. J.*, **276**, 284.
Marilli, E. & Catalano, S., 1984. *Astr. Astrophys.*, **133**, 57.
Mewe, R. & Gronenschild, E. H. B. M., 1981. *Astr. Astrophys. Suppl.*, **45**, 11.
Neupert, W. M., 1965. *Ann. d'Astrophys.*, **28**, 446.
Noyes, R. W., Hartmann, L., Baliunas, S. L., Duncan, D. K. & Vaughan, A. H., 1984. *Astrophys. J.*, **279**, 763.
Nussbaumer, H. & Storey, P. J., 1984. *Astr. Astrophys.*, **140**, 383.
Oranje, B. J., 1986. *Astr. Astrophys.*, **154**, 185.
Pallavicini, R, Golub, L., Rosner, R. & Vaiana, G., 1981. *Proc. Second Work Shop on Cool Stars, Stellar System & the Sun, SAO Special Report, No. 39*, 2, Vol. II, p. 77.
Raymond, J. C., Cox, D. P. & Smith, B. W., 1976. *Astrophys. J.*, **204**, 209.
Robinson, R. D., Worden, S. P. & Harvey, J. W., 1980. *Astrophys. J.*, **236**, L155.
Rosner, R., Tucker, W. H. & Vaiana, G. S., 1978. *Astrophys. J.*, **220**, 643.
Saar, S. H., Linksy, J. L. & Beckers, J. M., 1986. *Astrophys. J.*, **302**, 777.
Saar, S. H., Linsky, J. L. & Duncan, D. K., 1986. In: *Cool Stars, Stellar Systems and the Sun*, p. 275, eds Zeilik, M. & Gibson, D. M., Springer-Verlag, Berlin.
Schrijver, C. J., Mewe, R. & Walter, F. M., 1984. *Astr. Astrophys.*, **138**, 258.
Serio, S., Peres, G., Vaiana, G. S., Golub, L. & Rosner, R., 1981. *Astrophys. J.*, **243**, 288.
Simon, T., Herbig, G. & Boesgaard, A. M., 1985. *Astrophys. J.*, **293**, 551.
Simon, T., Kelch, W. L. & Linsky, J. L., 1980. *Astrophys. J.*, **237**, 72.
Smith, G., Edvardsson, B. & Frisk, U., 1986. *Mon. Not. R. astr. Soc.*, in press.
Stein, R. F., 1981. *Astrophys. J.*, **246**, 966.
Stencel, R. E., Mullan, D. J., Linsky, J. L., Basri, G. S. & Worden, S. P., 1980. *Astrophys. J. Suppl.*, **44**, 383.

Summers, H. P. & McWhirter, R. W. P., 1979. *J. Phys. B.,* **12,** 2387.
Tatum, J., 1968. *Mon. Not. R. astr. Soc.,* **140,** 87.
Ulmschneider, P. & Stein, R. F., 1982. *Astr. Astrophys.,* **106,** 9.
Vernazza, J. E., Avrett, E. H. & Loeser, R., 1981. *Astr. Astrophys. Suppl.,* **45,** 635.
Walter, F. M., 1981. *Astrophys. J.,* **245,** 677.
Walter, F. M., 1982. *Astrophys. J.,* **253,** 745.
Walter, F. M., Linsky, J. L., Bowyer, C. S. & Garmire, G., 1980. *Astrophys. J.,* **236,** L137.
Walter, F. M., Linsky, J. L., Simon, T., Golub, L. & Vaiana, G. S., 1984. *Astrophys. J.,* **281,** 815.
Weiler, E. J. & Oergerle, W. R., 1979. *Astrophys. J. Suppl.,* **39,** 537.